Biochemical Journal (2020) **477** 2153–2177
https://doi.org/10.1042/BCJ20200145

PORTLAND PRESS

Research Article

Molecular dynamics simulations and biochemical characterization of *Pf*14-3-3 and *Pf*CDPK1 interaction towards its role in growth of human malaria parasite

Ravi Jain[1], Pinki Dey[2], Sakshi Gupta[3], Soumya Pati[1], Arnab Bhattacherjee[2], Manoj Munde[3] and Shailja Singh[1,4]

[1]Department of Life Sciences, School of Natural Sciences, Shiv Nadar University, Gautam Buddha Nagar, UP 201314, India; [2]School of Computational and Integrative Sciences, Jawaharlal Nehru University, Delhi 110067, India; [3]School of Physical Sciences, Jawaharlal Nehru University, Delhi 110067, India; [4]Special Centre for Molecular Medicine, Jawaharlal Nehru University, Delhi 110067, India

Correspondence: Shailja Singh (shailja.jnu@gmail.com)

Scaffold proteins play pivotal role as modulators of cellular processes by operating as multipurpose conformation clamps. 14-3-3 proteins are gold-standard scaffold modules that recognize phosphoSer/Thr (*p*S/*p*T) containing conserved motifs, and confer conformational changes leading to modulation of functional parameters of their target proteins. Modulation in functional activity of kinases has been attributed to their interaction with 14-3-3 proteins. Herein, we have annotated and characterized PF3D7_0818200 as 14-3-3 isoform I in *Plasmodium falciparum* 3D7, and its interaction with one of the key kinases of the parasite, Calcium-Dependent Protein Kinase 1 (CDPK1) by performing various analytical biochemistry and biophysical assays. Molecular dynamics simulation studies indicated that CDPK1 polypeptide sequence (^{61}KLG*p*S^{64}) behaves as canonical Mode I-type (RXX*p*S/*p*T) consensus 14-3-3 binding motif, mediating the interaction. The 14-3-3I/CDPK1 interaction was validated *in vitro* with ELISA and SPR, which confirmed that the interaction is phosphorylation dependent, with binding affinity constant of 670 ± 3.6 nM. The interaction of 14-3-3I with CDPK1 was validated with well characterized optimal 14-3-3 recognition motifs: Mode I-type ARSH*p*SYPA and Mode II-type RLYH*p*SLPA, by simulation studies and ITC. This interaction was found to marginally enhance CDPK1 functional activity. Furthermore, interaction antagonizing peptidomimetics showed growth inhibitory impact on the parasite indicating crucial physiological role of 14-3-3/CDPK1 interaction. Overall, this study characterizes 14-3-3I as a scaffold protein in the malaria parasite and unveils CDPK1 as its previously unidentified target. This sets a precedent for the rational design of 14-3-3 based PPI inhibitors by utilizing 14-3-3 recognition motif peptides, as a potential antimalarial strategy.

Introduction

Received: 18 February 2020
Revised: 28 May 2020
Accepted: 2 June 2020

Accepted Manuscript online: 2 June 2020
Version of Record published: 22 June 2020

Cellular signal transduction pathways often involve Post-Translational Modifications (PTMs) of proteins which influence their overall spatial 3D-conformation, thereby affecting their stability, activity, and/or cellular localization [1]. Reversible phosphorylation of serine, threonine or tyrosine residues has been the most extensively studied PTM [2]. However, very often, phosphorylation is not solitary responsible for the modulation of protein function. Rather, phosphorylation of a protein mediates its interaction with downstream interacting partners, which ultimately regulates protein function. 14-3-3 proteins serve as prototype for a novel class of scaffold modules that recognize phosphor-Ser/Thr (*p*S/*p*T)

PORTLAND PRESS

Biochemical Journal (2020) **477** 2153–2177
https://doi.org/10.1042/BCJ20200145

containing conserved motifs in a variety of proteins. 14-3-3s are highly evolutionarily conserved small, dimeric (homo- and heterodimers) and acidic proteins that are widespread in almost all eukaryotic organisms [3–5]. Whereas yeast has two genetically distinct but structurally homologous isoforms, and mammals seven, most plant genomes contain a dozen 14-3-3 genes which can be divided into two distinct groups: *epsilon* and *non-epsilon*, based on their sequence homology and exon/intron structure [3,4,6,7]. Although high degree of sequence similarity among 14-3-3 isoforms suggests functional redundancy, the presence of phenotypes for single and multiple 14-3-3 knock-out mutants suggest that 14-3-3 isoforms *selectively* bind to their *individual* protein ligands with *different* affinities, owing to the spatiotemporal regulation of expression of these isoforms [8–12]. Moreover, large number of 14-3-3 isoforms expressed in an organism suggests high combinatorial complexity in dimer re-arrangement, which in turn fine-tunes their cellular functions.

14-3-3 proteins often interact with their target proteins through canonical phosphorylated motifs, categorized as: Mode I (RXX*p*S/*p*T), Mode II (RXXX*p*S/*p*T) and Mode III (RXX*p*S/*p*TX_{1-2}C′), where X is any amino acid and *p*S/*p*T represents phosphoSer or phosphoThr [13–18]. The interaction is mediated by conserved amphipathic groove harbored by 14-3-3 [19,20]. Docking site for 14-3-3 is created by a combination of inherent shape and phosphate-group added in the target protein, in response to a particular signaling cascade [21]. In this context, the stability of 14-3-3 has been put forward as a basis for '*molecular anvil hypothesis*' in which the rigid 14-3-3 dimer mechanically imposes structural rearrangements in its target phosphorylated protein, thus regulating its functional properties, while itself undergoing only minimal structural alterations [22]. Depending on biochemical nature of the phosphorylated target protein(s), physical association with 14-3-3 can have different functional consequences, resulting either in modulation of their enzymatic activities, subcellular localization, stability or macromolecular interactions [4,11,23–28].

14-3-3 proteins, thus, operate as multipurpose *conformation (allosteric) clamps* which are recruited to hold their phosphorylated protein partner(s) in place, in response to cellular signaling pathways. The interaction with 14-3-3 culminates in the regulation of cellular functions like apoptosis, adhesion-dependent integrin signaling, cell cycle control in response to genotoxic stress, ion-channels functioning, etc., thus, governing diverse physiological processes and cellular status [4,24–27]. Studies on 14-3-3/client-protein interactions, by utilizing various biochemical and biophysical approaches, may therefore, provide tremendous opportunities for therapeutic interventions under numerous pathological conditions.

In the malaria parasite, *P. falciparum*, two 14-3-3 isoforms have been annotated by database curators based on sequence similarity with experimentally annotated orthologs: *Pf*14-3-3I and *Pf*14-3-3II (accession numbers: PF3D7_0818200 and PF3D7_1362100, respectively), as documented in Plasmodium Genomic Resource database (PlasmoDB; release 46; updated on 6th Nov., 2019; https://plasmodb.org/plasmo/). In the present study, we confirm the presence of 14-3-3 protein in the malaria parasite. Furthermore, we report that *Pf*14-3-3I interacts with a highly expressed protein in the parasite, Calcium-Dependent Protein Kinase 1 (CDPK1) that plays key role in multitude of essential cellular processes, including parasite invasion and egress during intra-erythrocytic proliferative stages of the parasite. Antagonizing the *Pf*14-3-3I/*Pf*CDPK1 protein–protein interaction (PPI), by using well characterized 14-3-3 recognition motifs, inhibits parasite growth *in vitro*, which indicates crucial physiological role of this PPI in the parasite. Our work sets a precedent for the rational design of 14-3-3 based PPI inhibitors, by utilizing 14-3-3 recognition motif peptides as a potential antimalarial strategy.

Materials and methods

Unless stated, all materials were purchased from Sigma–Aldrich, St Louis, MO, U.S.A.

Peptides

Two different phosphopeptides: Mode I (ARSH*p*SYPA or *peptide 1*) and Mode II (RLYH*p*SLPA or *peptide 2*) (*p*S: phosphoserine) were utilized to antagonize *Pf*14-3-3/*Pf*CDPK1 PPI inhibition. These phosphopeptides were identified by Rittinger et al. [29] from oriented peptide library screening and are recognized by all mammalian and *S. cerevisiae* 14-3-3 isotypes. The peptides (HPLC purity >98%) were synthesized from Biochain Incorporated, India. The HPLC and Mass spectrometry analysis reports for both peptides are provided in Supplementary File S2.

Culture of *P. falciparum* 3D7

Cryopreserved *P. falciparum* parasites (3D7 laboratory strain) were thawed and cultured according to the protocol as described by Trager and Jensen [30]. Briefly, parasite cultures were maintained in O^+ erythrocytes at 2% hematocrit level, in RPMI 1640 medium (Gibco®, U.S.A.) supplemented with 0.5% AlbuMAX™ I (Gibco®, U.S.A.),

50 mg/L hypoxanthine, 10 mg/L gentamycin (Gibco®, U.S.A.) and 2 gm/L sodium bicarbonate. Parasite culture was maintained in ambient hypoxic environment (5% O_2 and 5% CO_2; balanced with N_2). Prior to setting up an experiment, parasite culture was tightly synchronized at ring stage by lysing erythrocytes parasitized with mature parasites, with 5% sorbitol, for two successive intra-erythrocytic proliferative cycles of the parasite.

Comparative sequence analysis and domain architecture of *Pf*14-3-3I

Multiple Sequence Alignment (MSA) was performed on comprehensive ensembles of 14-3-3 protein sequences for contextualizing the patterns of conservation and correlation in *Pf*14-3-3I protein, in light of the structurally and functionally well-characterized 14-3-3 orthologs in humans. Amino acid sequences of 14-3-3 isoforms from *Homo sapiens* (seven isoforms: 14-3-3 epsilon, P62258; beta/alpha, P31946; zeta/delta, P63104; theta, P27348; gamma, P61981; eta, Q04917 and sigma, P31947) and *P. falciparum* strain 3D7 (two isoforms: *Pf*14-3-3I, PF3D7_0818200 and *Pf*14-3-3II, PF3D7_1362100) were retrieved from Universal Protein Resource Knowledgebase (UniProtKB; https://www.uniprot.org/) and PlasmoDB, respectively [31,32]. MSA was performed by using MultAlin tool, which creates sequence (either protein or nucleic acid) alignment from a group of related sequences by using progressive pairwise alignments. (http://multalin.toulouse.inra.fr/multalin/) [33]. Based on literature review, and comparative sequence analysis with the *Hs*14-3-3 isoforms, probable amino acid residues of *Pf*14-3-3I involved in dimerization and phosphopeptide (target) binding were employed to illustrate overall *Pf*14-3-3I architecture [25,29,34–36]. This was done by using Illustrator for Biological Sequences (IBS 1.0.3), a tool for visualizing biological sequences (http://ibs.biocuckoo.org/) [37].

Phylogenetic analysis and 14-3-3 binding consensus motifs

Phylogenetic relationship of *Pf*14-3-3 isoforms with their orthologs present across all three kingdoms of life: animalia, plantae and fungi, was established. To obtain full-length 14-3-3 protein sequences, BLASTp (https://blast.ncbi.nlm.nih.gov/Blast.cgi) search was performed by using amino acid sequence of *Pf*14-3-3I protein as *query sequence*, and whole proteomes of metazoans (taxid: 33208), embryophytes (taxid:3193) and fungi (taxid:4751) as *search sets*. Publicly available databases such as UniprotKB and The Arabidopsis Information Resource (https://www.arabidopsis.org/) were utilized to retrieve 14-3-3 protein sequences from *Homo sapiens* and *Arabidopsis thaliana*, respectively [31,38]. Literature survey was done to identify 14-3-3 proteins from *Saccharomyces cerevisiae,* and certain plant species including *Solanum lycopersicum*, *Populus trichocarpa*, *Oryza sativa*, *Glycine max* and *Medicago trucatula* [39–41]. 14-3-3 protein sequences, thus retrieved, from the BLASTp search, databases and literature survey (Supplementary File S1) were further categorized into two groups: *epsilon* and *non-epsilon*. Unrooted phylogenetic relationship of *Pf*14-3-3 isoforms with these orthologs was established by using MEGA6, a user-friendly software suite for analyzing DNA and protein sequence data from species and populations (http://www.megasoftware.net/) [42].

To identify experimentally validated 14-3-3 interacting proteins from prokaryotes and eukaryotes, and further collate details of their 14-3-3 binding phosphoSer/Thr sites, literature survey followed by mining of publically available databases was done. The Eukaryotic Linear Motif resource (ELM), a database of experimentally validated eukaryotic linear motifs (http://elm.eu.org/), and ANnotation and Integrated Analysis of the 14-3-3 interactome database (ANIA) which integrates multiple data sets on 14-3-3 binding phosphoproteins (https://ania-1433.lifesci.dundee.ac.uk/prediction/webserver/index.py) were used for this purpose [43,44]. The repertoire of experimentally determined gold-standard 14-3-3 binding phosphosites was further extended from the literature survey [45–47]. Amino acid sequences of these 14-3-3 binding phosphopeptides were used to *update* consensus 14-3-3 recognition motifs by using WebLogo 3, a web based application designed to generate sequence logos (http://weblogo.berkeley.edu/) [48]. Key protein kinases of the parasite (CDPK1, PKG, PKA_R and PKA_C) were filtered out as putative binding partners of *Pf*14-3-3I by combining 14-3-3 binding *motifs search* and global phosphoproteomic datasets of *p*S/*p*T peptides enriched from schizont stage of *P. falciparum* [49–53]. Overall domain architectures of the protein kinases were drawn by using IBS 1.0.3 [37].

cDNA preparation, molecular cloning, overexpression and purification of recombinant *Pf*14-3-3I and *Pf*CDPK1

cDNA from *P. falciparum* schizonts was prepared by following a previously described protocol, in the absence and presence of Reverse Transcriptase (RT) [54]. Integrity of cDNA, thus obtained, was checked by amplification of transcript encoding for 18s rRNA using the following primer sets: *18s*_Fwd, 5′-CCGCCCG

Biochemical Journal (2020) 477 2153–2177
https://doi.org/10.1042/BCJ20200145

TCGCTCCTACCG-3′ and *18s*_Rev, 5′-CCTTGTTACGACTTCTCCTTCC-3′. 18s rRNA was also amplified from genomic DNA (gDNA) of the parasite, as positive control. Presence of *Pf14-3-3I* transcripts in the cDNA pool was confirmed by amplification using the following primer sets: *pf14-3-3I*_Fwd, 5′-ATGGCAACATCTG AAGAATTAAAACA-3′ and *pf14-3-3I*_Rev, 5′-TTCTAATCCTTCGTCTTTTGATTTT-3′. *pf14-3-3I* gene was also amplified from gDNA of the parasite, as positive control. The experiment was done twice. Transcript encoding full-length *Pf*14-3-3I protein was amplified using the following primer sets: *Pf14-3-3I*_Fwd, 5′-TGCG GGATCCATGGCAACATCTGAAGAATTAAAACA-3′ and *Pf14-3-3I*_Rev, 5′-ATTTGTCGACTCATTCTAATC CTTCGTCTTTTGATT-3′, by using Phusion high-fidelity DNA polymerase (Thermo Scientific). Amplified DNA fragment encoding *Pf*14-3-3I was cloned between BamHI and SalI restriction sites of the expression vector pGEX-4T-1 vector (with a cleavable Glutathione S-Transferase tag at the N-terminus). Recombinant plasmid was transformed into *Escherichia coli* DH5α competent cells, and positive clones were confirmed by restriction digestion and Sanger sequencing of insert DNA fragment.

For overexpression of GST-*Pf*14-3-3I fusion protein, the recombinant plasmid containing *pf14-3-3I* gene was transformed into *E. coli* strain Rosetta competent cells. Overexpression of the protein was induced with 0.5 mM IsoPropyl β-D-1-ThioGalactopyranoside (IPTG) at 0.4–0.5 Optical Density (OD; at 600 nm) of bacterial secondary culture, for 8 h at 25°C. Cells were harvested by centrifugation at 4000***g*** in Sorvall® Evolution™ RC Centrifuge (Thermo Fisher Scientific ™) at 4°C for 15 min. Bacterial pellet, thus obtained, was resuspended in cell lysis buffer (buffer A) containing 10 mM HEPES-NaOH, pH 7.4; 1 mM Ethylene Diamine Tetraacetic Acid (EDTA); 150 mM NaCl; 25 μg/ml lysozyme; 3 mM β-MercaptoEthanol (βME), Protease Inhibitor Cocktail (PIC, Roche) and 1 mM PhenylMethylSulfonyl Fluoride (PMSF), followed by sonication for 15 min with successive pulses of 6 s ON and 10 s OFF. Cell lysate was centrifuged at 15,000 ***g***, at 4°C for 1 h. Supernatant, thus obtained, was loaded onto Glutathione Sepharose High Performance resin packed column, GSTrap™ HP 1 ml (GE Healthcare) pre-equilibrated with buffer B (10 mM HEPES-NaOH, pH 7.4; 1 mM EDTA and 150 mM NaCl), for overnight at 4°C. After protein binding, the column was washed with 10 fold column volume of buffer B and recombinant 14-3-3I protein was eluted with different concentrations (10, 20 and 50 mM) of reduced glutathione, prepared in buffer B. Elution fractions, thus obtained, from affinity purification were pooled and buffer exchanged using Amicon™ Ultra-15 Centrifugal Filter Unit (10 kDa cutoff; Merck™) in 10 mM HEPES-NaOH buffer (pH 7.4) and 150 mM NaCl.

To raise specific antibodies against r14-3-3I protein, four female Balb/c mice (6 to 8 weeks old) were each administered (i.p.) with 50 μg of the recombinant protein (in 0.9% saline), in a prime and boost regimen. For priming dose (day 0), the formulation was made by thoroughly mixing equal volumes of Freund's complete adjuvant and saline containing the protein. For subsequent booster doses (days 21 and 42), formulations were made with Freund's incomplete adjuvant. Blood samples were collected from retro-orbital sinus of the mice on days 31 and 52 (terminal bleed) after primary immunization. Collected blood samples were incubated for 30 min at 37°C, centrifuged at 1200×***g*** at 4°C for 15 min, and then serum samples were collected and stored at −80°C until further analysis. Once the antiserum was raised, native *Pf*14-3-3I protein was detected in schizonts lysate by immunoblotting. The experiment was done twice.

Cloning of *pfcdpk1* gene in pET-28a(+) vector (with 6x-His tags at N- and C-termini) was done as described earlier [54]. For overexpression of 6x-His-*Pf*CDPK1 fusion protein, the recombinant plasmid harboring *pfcdpk1* gene was transformed into *E. coli* strain BLR (λDE3) competent cells. Overexpression of the protein was induced with 1 mM IPTG at 0.9 OD of bacterial secondary culture, for 4 h at 30°C. Protein purification was done in a similar manner as described above for the purification of r14-3-3I, except for the following changes in buffers' compositions: buffer A: 10 mM Tris, pH 8.0; 1 mM EDTA; 100 mM NaCl; 25 μg/ml lysozyme; 3 mM βME and PIC; and, buffer B: 10 mM imidazole; 10 mM Tris, pH 8.0; 100 mM NaCl and 3 mM βME. Supernatant obtained after centrifugation of bacterial lysate was loaded onto High-Performance Immobilized Metal Affinity Chromatography (IMAC) column, HisTrap™ HP 1 ml (GE Healthcare) and rCDPK1 protein was eluted with different concentrations of imidazole ranging from 20–500 mM, prepared in buffer B. Elution fractions, thus obtained, from metal-affinity purification were pooled and buffer exchanged, as mentioned above for r14-3-3I protein.

Immuno-Fluorescence assay (IFA) to detect expression and co-localization of *Pf*14-3-3I with *Pf*CDPK1

IFAs were performed on synchronized *P. falciparum* 3D7 culture to check for expression of *Pf*14-3-3I and its co-localization with *Pf*CDPK1 in mature stages of the parasite, as described earlier [55]. Briefly, mature

schizonts (44–46 hpi) and merozoites were isolated, smeared on glass slides, dried and fixed with pre-chilled methanol for overnight at −20°C. Non-specific binding sites in the parasite were blocked with 3% BSA (in 1× PBS), for 1 h at room temperature (RT, 293 K) and probed with anti-*Pf*14-3-3I mouse serum and anti-*Pf*CDPK1 rabbit serum at dilutions of 1 : 50, for 1 h at RT. Slides were washed twice with PBS containing 0.05% Tween-20 (PBST), followed by washing once with PBS, and probed with Alexa-Fluor 488 conjugated anti-mouse IgG (Molecular Probes, U.S.A.) and Alexa-Fluor 594 conjugated anti-rabbit IgG, both at dilutions of 1 : 500, for 1 h at RT. All antibodies were diluted in 1% BSA, prepared in 1X PBS. The slides were washed and mounted with ProLong Gold antifade reagent with DAPI (4′,6- diamidino-2-phenylindole; Invitrogen). Images were acquired in Olympus FLUOVIEW FV3000 confocal microscope using Olympus cellSens dimensions imaging software. Expression and Co-localization analysis from all three channels (blue: DAPI; green: *Pf*14-3-3I; red: *Pf*CDPK1) was performed on a pixel by pixel basis using the same software. Every pixel in the image was plotted in the scatter diagram based on its intensity level from the channels, followed by estimation of Pearson's correlation coefficient, *r*. For the estimation of '*r*', an infected and stained RBC was selected using the Region of Interest (ROI) tool provided in the software. From this ROI area, the '*r*' value was noted as given by the software in ROI statistics [55]. The experiment was done thrice.

Homology modeling of *Pf*14-3-3I and *Pf*CDPK1

Three-dimensional structure of a protein can provide us with precise information about its single, most stable conformation, as dictated by its sequence. Comparative or homology modeling, one of the most common structure prediction methods in structural genomics and proteomics, was employed to model 3D structures of *Pf*14-3-3I$_{dimer}$ and *Pf*CDPK1 from *P. falciparum* strain 3D7. To accomplish this feat, amino acid sequences of *Pf*14-3-3I (PF3D7_0818200) and *Pf*CDPK1 (PF3D7_0217500) were retrieved from PlasmoDB database [32]. To search for a suitable template for homology modeling, BLASTp (https://blast.ncbi.nlm.nih.gov/Blast.cgi) search was performed by using amino acid sequences of *Pf*14-3-3I and *Pf*CDPK1 as *query sequences*, against Protein Data Bank (PDB) database (http://www.rcsb.org/) [56,57]. Amino acid sequence identity between 14-3-3 orthologs from *P. falciparum* strain 3D7 (14-3-3I) and *Homo sapiens* (14-3-3 Epsilon) was found to be 63.52%, thus, rendering X-Ray diffraction based structural model of *Hs*14-3-3 epsilon (PDB ID: 3UAL; resolution: 1.8 Å) as a suitable template to model 3D structure of *Pf*14-3-3I$_{dimer}$ [58]. For *Pf*CDPK1, X-ray diffraction based structural model of CDPK1 protein from *P. berghei* strain ANKA (PDB ID: 3Q5I; sequence similarity: 93%) was used as a suitable template, as described previously by our group [59,60]. Homology modeling was done by using Modeller v9.17 software (https://salilab.org/modeller/), a program designed for comparative protein structure modeling by satisfaction of spatial restraints [61]. The best structural model with the most negative DOPE score was selected and rendered with PyMOL Molecular Graphics System, v2.1 by Schrödinger, LLC (http://pymol.org/2/) [62].

Generated models were further subjected to structural refinement by using ModRefiner (https://zhanglab.ccmb.med.umich.edu/ModRefiner/) which is an algorithm-based approach for atomic-level, high-resolution protein structure refinement [63]. Reliability of the refined structural models of *Pf*14-3-3I$_{dimer}$ and *Pf*CDPK1 was assessed by examining backbone dihedral (torsion) angles: phi (Ø) and psi (Ψ) of the amino acid residues lying in the energetically *favorable* regions of Ramachandran space [64]. This was done by using PROCHECK v.3.5 (https://www.ebi.ac.uk/thornton-srv/software/PROCHECK/) [65]. Percent quality measurement of the protein structures was evaluated by using four sorts of occupancies called 'core', 'additional allowed', 'generously allowed' and 'disallowed' regions. The refined 3D structural models of *Pf*14-3-3I$_{dimer}$ and *Pf*CDPK1, thus generated, were subsequently used for *Pf*14-3-3I$_{dimer}$/*Pf*CDPK1 PPI and *Pf*14-3-3I$_{dimer}$/peptides interaction, and molecular dynamics simulation studies.

Molecular docking

Molecular docking of the structurally modeled phosphopeptides (*peptide 1*: ARSH*p*SYPA and *peptide 2*: RLYH*p*SLPA; *pS*: phosphorylated serine) against *Pf*14-3-3I$_{dimer}$ was performed by using AutoDock 4.2.6 tool (http://autodock.scripps.edu/) [66]. For the receptor *Pf*14-3-3I$_{dimer}$ protein, we assigned polar Hydrogen and Kollman charges, whereas Marsilli-Gasteiger partial charges were assigned for the peptides. We have not used any additional restraint on torsion angles of the receptor protein during the docking process. The Lamarckian Genetic Algorithm (LGA) was used for performing the energy evaluations with a default set of docking parameters. All the docked complexes were evaluated based on their lowest binding energy (kcal/mol).

Biochemical Journal (2020) 477 2153–2177
https://doi.org/10.1042/BCJ20200145

*Pf*CDPK1 was docked against *Pf*14-3-3I$_{dimer}$ receptor by using High Ambiguity Driven biomolecular DOCKing (HADDOCK) webserver, an information-driven flexible docking approach for the modeling of biomolecular complexes [67]. We preferentially selected those Ser/Thr residues that were previously reported to be autophosphorylated by *Pf*CDPK1 [68]. To phosphorylate them *in silico*, we adopted the PyTMs plugin in PyMOL Molecular Graphics System [69]. During the whole docking process, the phosphorylated Ser/Thr residues present at the interface of *p*CDPK1 and *Pf*14-3-3I$_{dimer}$ receptor were considered as *active* residues, and amino acid residues surrounding those as *passive* residues.

Molecular dynamics (MD) simulation

Preparation and parameterization

*Pf*14-3-3I$_{dimer}$/*p*CDPK1 and *Pf*14-3-3I$_{dimer}$/peptides complex systems were parameterized by using terminal interface, *tLeap* of Assisted Model Building with Energy Refinement tool, AMBER 14 [70]. The system was neutralized by using the counter-charged ions (Na^+ or Cl^-) followed by solvation using explicit TIP3P water model spanning for 12 Å around the complex systems. The Forcefield *ff03.r1* was used for the proteins and peptides, and the phosphorylated Ser and Thr residues were handled by using the *ffptm* force filed [71,72].

Simulation

*Pf*14-3-3I$_{dimer}$/*p*CDPK1 and *Pf*14-3-3I$_{dimer}$/peptides complex systems were equilibrated by carrying out a short minimization (1000 steps, 500 cycles of steepest descent and 500 cycles of conjugate gradient minimization) runs followed by 50 ps of heating, 50 ps of density equilibration and 500 ps of constant pressure equilibration, performed at 300 K. During the equilibration process, the bonds involving Hydrogen-atoms were handled by SHAKE algorithm [73]. The simulations were carried out at 1 fs time step with Langevin thermostat, under the 'periodic boundary conditions' using *sander*, an AMBER 14 module which carries out energy minimization, molecular dynamics, and NMR refinements.

After the equilibration, production runs were performed at 300 K with Langevin thermostat, under a constant pressure. We performed 20 ns long simulations for *Pf*14-3-3I$_{dimer}$/peptides complexes and 100 ns long simulation for *Pf*14-3-3I$_{dimer}$/*p*CDPK1 complex, and the co-ordinates were updated after every 5 ps. We used a non-bonded cutoff distance of 8 Å, and Particle Mesh Ewald (PME) algorithm handled the long ranged electrostatic interactions [74]. The net translational and rotational velocities were canceled after every 1000 steps. The simulations were carried out at 1 fs time step by using *pmemd*, a version of *sander* that is optimized for speed and parallel scaling.

Analysis and binding energy calculation

Residue specific free energy decomposition was performed by using Molecular Mechanics/Generalized Born and Surface Area (MM/GBSA) continuum solvation method [75]. Here, we calculated Gibbs free energy of binding (ΔG_{bind}) for both *Pf*14-3-3I$_{dimer}$/peptides and *Pf*14-3-3I$_{dimer}$/*p*CDPK1 interactions, as follows:

$$\Delta G_{bind} = G_{complex} - (G_{receptor} + G_{ligand}) \quad (1)$$

Where, Gibbs free energy is the sum of:

$$\Delta G_{bind} \approx \Delta E_{internal} + \Delta E_{ele} + \Delta E_{vdW} + \Delta G_{pol} + \Delta G_{np} - T\Delta S \quad (2)$$

Where, $\Delta E_{internal}$ includes bond, bend and dihedral energies of the system; ΔE_{ele} and ΔE_{vdW} denote electrostatic and Van Der Waals interaction energies, respectively; ΔG_{pol} and ΔG_{np} denote polar and non-polar solvation terms, respectively. The polar solvation term was calculated by Generalized Born (GB) model, whereas the non-polar solvation term was calculated from linear relation to the solvent accessible surface area. $T\Delta S$ is the product of temperature and entropy terms. We used MMPBSA.py.MPI module of AMBER 14 to calculate ΔG_{bind} for both *Pf*14-3-3I$_{dimer}$/peptides and *Pf*14-3-3I$_{dimer}$/*p*CDPK1 interaction systems by using MM/GBSA method [76].

Autophosphorylation of *Pf*CDPK1 *in vitro*

*Pf*CDPK1 phosphorylation was achieved by setting up a kinase reaction *in vitro* with 100 ng/µl of rCDPK1 in assay buffer [100 mM Tris–Cl, pH 7.4; 2.5 mM DiThioThreitol (DTT); 50 mM $MgCl_2$ and 2.5 mM $MnCl_2$].

Enzymatic reaction was carried out in a total volume of 200 μl, in the absence and presence of Ca^{2+}-ions for conditions requiring minimally (represented as rCDPK1) and maximally (represented as r*p*CDPK1) phosphorylated *Pf*CDPK1 protein, respectively. An amount of 2.5 mM EGTA was added for condition requiring absence of Ca^{2+}-ions. Kinase reactions were initiated by adding 1 mM ATP and allowed to take place at 30°C for 1 h. Auto-phosphorylation status of *Pf*CDPK1 was confirmed by in-gel fluorescence staining with phosphoamino acid stain, Pro-Q Diamond (Thermo Fisher Scientific™). Protocol was followed as recommended by the supplier. Briefly, SDS–PAGE was performed for the phosphorylation reactions carried out in the absence and presence of Ca^{2+}-ions. 10 μg each of rCDPK1 and r*p*CDPK1 was loaded onto gel lanes. Phosphostained gels were imaged using Molecular Imager® Pharos FX™ Systems (Bio-Rad). Excitation was set at 555 nm with emission filter of 580 BP 30. Estimates of band intensities of rCDPK1 and r*p*CDPK1 from phosphostained gel images were made using ImageJ 1.52a, which is a public domain Java image processing program. Lanes and bands were auto-detected and manually size-adjusted to ensure full band inclusion and equivalent thickness across all lanes. In all subsequent experiments, minimally and maximally phosphorylated *Pf*CDPK1 protein is represented as rCDPK1 and r*p*CDPK1, respectively.

*Pf*CDPK1 enzymatic activity *in vitro*

Phosphorylation experiments were performed with 100 ng of rCDPK1, per reaction, in assay buffer (100 mM Tris–Cl, pH 7.4; 2.5 mM DTT; 50 mM $MgCl_2$ and 2.5 mM $MnCl_2$) by following protocol, as described previously by our group [60,77]. Enzymatic reaction was carried out in the absence and presence of Ca^{2+}-ions. An amount of 10 μg of dephosphorylated casein from bovine milk, per reaction, was used as exogenous substrate for the enzyme. An amount of 2.5 mM EGTA was added for conditions requiring absence of Ca^{2+} ions. Kinase reactions were initiated by adding 1 mM ATP and allowed to take place at 30°C for 1 h. To test for any regulatory effect of *Pf*14-3-3I on the functional activity of *Pf*CDPK1, rCDPK1 was allowed to pre-incubate with equivalent amount of r14-3-3I in the reaction buffer, at room temperature for 1 h, followed by initiating the reaction with the addition of ATP. After completion of the reactions, phosphorylation status of *Pf*CDPK1 and casein was checked by in-gel fluorescence staining with phosphoamino acid stain, Pro-Q Diamond (Thermo Fisher Scientific™). Protocol was followed as described above to confirm autophosphorylation of CDPK1. The experiment was done twice.

ELISA to confirm *Pf*14-3-3I/*Pf*CDPK1 interaction

ELISA was performed to confirm *Pf*14-3-3/*Pf*CDPK1 interaction, by following previously described protocol [78]. Briefly, purified *Pf*CDPK1 protein (200 ng/100 μl/well of rCDPK1 or r*p*CDPK1) was coated onto Poly-L-Lysine treated 96-welled microtitre plate, in 0.06 M carbonate-bicarbonate buffer (pH 9.6), for overnight at 4°C. The plate was blocked with 5% skimmed milk solution (in PBS; 200 μl/well) for 1 h at 37°C and washed thrice with 0.05% Tween in PBS (PBST) for 5 min each. For interaction analysis, *Pf*CDPK1 coated wells were incubated with different concentrations of r14-3-3I protein: 0.5, 1, 2, 4 and 8 μM (100 μl/well), for 1 h at 37°C. Equivalent concentrations of GST were taken as negative controls. Following three washes with PBST, anti-GST HRP Conjugated antibody (Sigma–Aldrich; diluted 1 : 5000 in PBS) was added to each well (100 μl/well) and incubated for 1 h at 37°C. The peroxidase reaction was developed with o-Phenylenediamine Dihydrochloride (OPD; 1 mg/ml) as chromogen and hydrogen peroxide as substrate, both prepared in citrate phosphate buffer, pH 5.0 (100 μl/well). The enzymatic reaction was stopped with 2N H_2SO_4 and the optical density was measured spectrophotometrically by taking absorbance at 490 nm using Varioskan™ LUX multimode microplate reader (Thermo Fisher Scientific™). For conditions requiring presence of peptides (1 or 2) as *Pf*14-3-3I/*Pf*CDPK1 interaction inhibitor, ELISA was performed in the presence of different concentrations of each peptide: 1, 5, 10, 25 and 50 μM. The experiment was done twice in triplicates.

Pull-down assay to confirm *Pf*14-3-3I/*Pf*CDPK1 interaction

To further confirm *Pf*14-3-3I/*Pf*CDPK1 interaction, western blot based GST pull-down assay was performed in which Glutathione Sepharose® 4B beads (GE Healthcare) were coupled with 10 μg of r14-3-3I in buffer A (20 mM Tris, pH 7.4; 0.5 mM DTT; 10 mM $MgCl_2$; 0.5 mM $MnCl_2$; 50 mM NaCl; 4% (v/v) glycerol; 0.1 mg/ml BSA and 25 mM $CaCl_2$), for 1 h at RT, followed by washing three times (at 900 rpm for 2 min.) with the same buffer. Equivalent amount of GST was taken as negative control. *Pf*CDPK1 was auto-phosphorylated in an *in vitro* kinase reaction, as mentioned above. r14-3-3I bound beads were incubated with *Pf*CDPK1 (10 μg of rCDPK1 or r*p*CDPK1, per binding reaction), for 1 h at RT. After washing three times with buffer B (buffer A

Biochemical Journal (2020) 477 2153–2177
https://doi.org/10.1042/BCJ20200145

with 300 mM NaCl), bead-bound protein complexes were boiled in SDS-loading dye and analyzed by SDS–PAGE, followed by immunoblotting with HRP-conjugated anti-His antibody (Sigma–Aldrich) by using SuperSignal™ West Femto Maximum Sensitivity Substrate (Thermo Scientific). The blot was stripped and re-probed with HRP-conjugated anti-GST antibody to check for equal coupling of r14-3-3I (or GST) with the beads in all binding reactions. For conditions requiring presence of peptides (1 or 2) as *Pf*14-3-3I/*Pf*CDPK1 interaction inhibitor, GST pull-down assay was performed in the presence of 10 μM concentration of each peptide. Two independent experiments were performed.

Surface plasmon resonance analysis of binding affinity between *Pf*CDPK1 and *Pf*14-3-3I

rCDPK1 protein was auto-phosphorylated in an *in vitro* kinase reaction, as mentioned above. To determine binding strength of *Pf*CDPK1/*Pf*14-3-3I complex, real-time biomolecular interaction analysis with Surface Plasmon Resonance (SPR) was carried out at physiologically relevant concentrations, by using AutoLab Esprit SPR (at Advanced Instrumentation Research Facility, Jawaharlal Nehru University, New Delhi, India). Kinetic rate constants: K_a and K_d (association and dissociation rate constants, respectively) as well as affinity constant, K_D were measured at RT. SPR analysis was performed by following previously described protocols [60,79–83]. Briefly, 5 μM of r14-3-3I was immobilized on the surface (self-assembled monolayer of 11-Mercapto-Undecanoic Acid, MUA on gold surface) of SPR sensor chip by the mechanism of *covalent amine coupling*. The chemistry involves covalent linkage of esterified carboxyl groups of the sensor surface with ε-amino group of lysine residues of a given protein. Unreacted ester groups on the sensor chip surface were blocked with 100 mM Ethanolamine, pH 8.5. Interaction kinetics was studied by injecting rCDPK1 or r*p*CDPK1 over the r14-3-3I immobilized chip surface at different concentrations: 100, 250, 500, 750 and 1000 nM, at a steady rate of 20 μl/min, with association and dissociation time of 300 s and 150 s, respectively. HEPES-NaOH buffer was used both as immobilization and binding solution. Surface of the sensor chip was regenerated with 50 mM NaOH. The experiment was done twice.

Data were fit to the two-state conformational change model by using AutoLab SPR Kinetic Evaluation software provided with the instrument. At least three independent experiments were performed. K_D value was calculated by using the Integrated Rate Law (IRL) equation:

$$R(t) = E.(1 - e^{Ks.t}) + R(0) \tag{3}$$

where, E is the maximal extent of change in response at a certain concentration and is equal to $k_a.C.R_{max}/(k_a.C + k_d)$; K_s is equal to $(k_a.C + k_d)$; and $R(0)$ is the response unit at $t = 0$. E and K_s were evaluated at each concentration by minimizing residual sum of squares between observed data and the model equation using solver in MS Excel. Evaluation of K_s at four different concentrations of the compounds was done to calculate K_D according to the following equation:

$$K_s = k_a.C + k_d \tag{4}$$

where, K_s is a concentration dependent parameter which is dependent upon k_a and k_d. Ratio of intercept (k_d) and slope (k_a) of the above line was ascertained to be the dissociation constant or K_D.

Isothermal titration calorimetric analysis

To calculate kinetic parameters such as binding affinity constant (K_a) associated with the interaction of r14-3-3I with peptides 1 and 2, Isothermal Titration Calorimetry (ITC) experiments were performed, by using MicroCal iTC200 (Malvern Instruments Ltd, UK; at School of Physical Sciences, Jawaharlal Nehru University, New Delhi, India). HEPES-NaCl buffer was degassed by vacuum for 10 min, prior to use. Dilutions of r14-3-3I and peptides were prepared in the degassed HEPES-NaCl buffer to ignore contribution from buffer-buffer interaction. ITC analysis was done at RT, by following previously described protocols [60,82,84,85]. Briefly, syringe was loaded with 40 μl of the ligand (i.e. peptide 1 or 2) at concentration of 40 μM (peptide 1) and 100 μM (peptide 2), and sample cell was filled with 280 μl of r14-3-3I at 10 μM concentration. Volume of first injection of the ligand was set to 0.4 μl, with an initial delay of 60 s. It was followed by 19 successive injections each of 2 μl, with an interval of 150 s between each injection to allow the signals to reach baseline.

Biochemical Journal (2020) 477 2153–2177
https://doi.org/10.1042/BCJ20200145

Background titration profiles were obtained by injecting ligand into the buffer solution, under identical experimental conditions. Heat of dilution of the ligand, thus obtained, was subtracted to determine net enthalpy change for r14-3-3I/peptides (1 or 2) interaction. The experiment was done twice. Amount of heat produced per injection (corrected data) was evaluated by integration of area under individual peaks by MicroCal ORIGIN 7 software provided by the instrument manufacturer. Experimental data was presented as the amount of heat produced per second (μcal/sec; corrected for heat of dilution of the ligand), following each injection of the ligand into the protein solution, as a function of time (minutes). Interaction data was represented as the best fit of the non-linear experimental data to a single-site binding model, yielding molar binding stoichiometry (N), binding constant (K_a), enthalpy change (ΔH) and entropy change (ΔS). Using K_a, ΔH and ΔS, the Gibbs free energy change (ΔG) was calculated by using the following equation:

$$\Delta G = \Delta H - T\Delta S = -\mathrm{RT}\ln K_a \quad (5)$$

Evaluation of growth inhibitory effect on malaria parasites

Peptides 1 and 2 were subjected to parasite invasion inhibition *in vitro* as described previously [86]. Briefly, mature (punctated) schizonts at 1% initial parasitaemia were treated with 12.5 μM concentration of the peptides, for 24 h at 37°C. Untreated parasites were taken as control. After progression of the parasites to ring stage, erythrocytes were washed with 1× PBS and stained with Ethidium Bromide (EtBr, 10 μM) for 20 min at RT, in dark. Following two washes with 1× PBS, cells were analyzed by flow cytometry on BD LSRFortessa™ cell analyzer using FlowJo v10 software. Fluorescence signal (FL-2) was detected with 590 nm band pass filter, by using an excitation laser of 488 nm, collecting 100 000 cells per sample. Following acquisition, parasitaemia levels were estimated by determining the proportion of FL-2-positive cells using Cell Quest. The experiment was done twice in triplicates. Percent parasite invasion inhibition was calculated as follows.

$$\%\ \text{Parasite invasion inhibition} = [1-(\%\ \text{Parasitaemia}_{(\text{treatment})}/\%\ \text{Parasitaemia}_{(\text{Control})})] \times 100 \quad (6)$$

Statistical analysis

In the bar graphs, data is expressed as Mean ± Standard Deviation (SD) of three independent experiments, done in duplicates. Statistical analysis was done by using OriginPro Evaluation 2018b Graphing and Analysis software. Unless indicated, the differences were considered to be statistically significant at $P < 0.05$; ns (not significant) indicates $P > 0.05$, one star indicates $P < 0.05$ and two stars indicate $P < 0.01$.

Results

Sequence analysis and identification of *Pf*14-3-3I

MultAlin-based sequence alignment of *Pf*14-3-3I with its well-characterized orthologs in humans demonstrated patterns of conservation and correlation in *Pf*14-3-3I (Figure 1a). Residues with high consensus value (>90%) are shaded in red and those with low consensus value (<90% and >50%) are shaded in blue. α-helices and Nuclear Export Signal (NES) are also indicated. Five highly conserved sequence blocks, as identified by Wang and Shakes [34] were observed, as shown boxed and shaded red. Residues at the dimerization interface (solid circles) and residues involved in phosphopeptide (target) binding (solid squares) were found to be conserved in all 14-3-3 isotypes, except *Pf*14-3-3II which appears to be the most divergent form of 14-3-3 proteins. Based on the literature review [25,29,34–36] and comparative sequence analysis with the *Hs*14-3-3 isoforms, probable amino acid residues of *Pf*14-3-3I involved in dimerization and phosphopeptide (target) binding were identified and highlighted in the overall *Pf*14-3-3I architecture (Figure 1b).

X-Ray diffraction based structural model of *Hs*14-3-3 epsilon$_{dimer}$ was used as a template to generate three-dimensional co-ordinates of *Pf*14-3-3I$_{dimer}$. After optimal rigid-body superimposition of the generated structural model of *Pf*14-3-3I$_{dimer}$ with *Hs*14-3-3 epsilon$_{dimer}$, overall Root-Mean-Square Deviation (RMSD) value of the C-alpha atomic co-ordinates was found to be 0.63 Å, suggesting a reliable 3D structure. *Pf*14-3-3I$_{dimer}$ homology model revealed strong resemblance with it's counterparts from other living organisms, with overall folds forming a clamp like structure, where each monomer is capable of forming a functional amphipathic groove for binding to phosphorylated residues (*p*S/*p*T) on target protein(s). Additionally, both monomers of *Pf*14-3-3I$_{dimer}$ were found to be oriented in opposite direction with respect to each other. Helical regions in one of the monomers of *Pf*14-3-3$_{dimer}$ are marked from H1 to H9 (Supplementary Figure S1a). Assessment of

PORTLAND PRESS

Biochemical Journal (2020) **477** 2153–2177
https://doi.org/10.1042/BCJ20200145

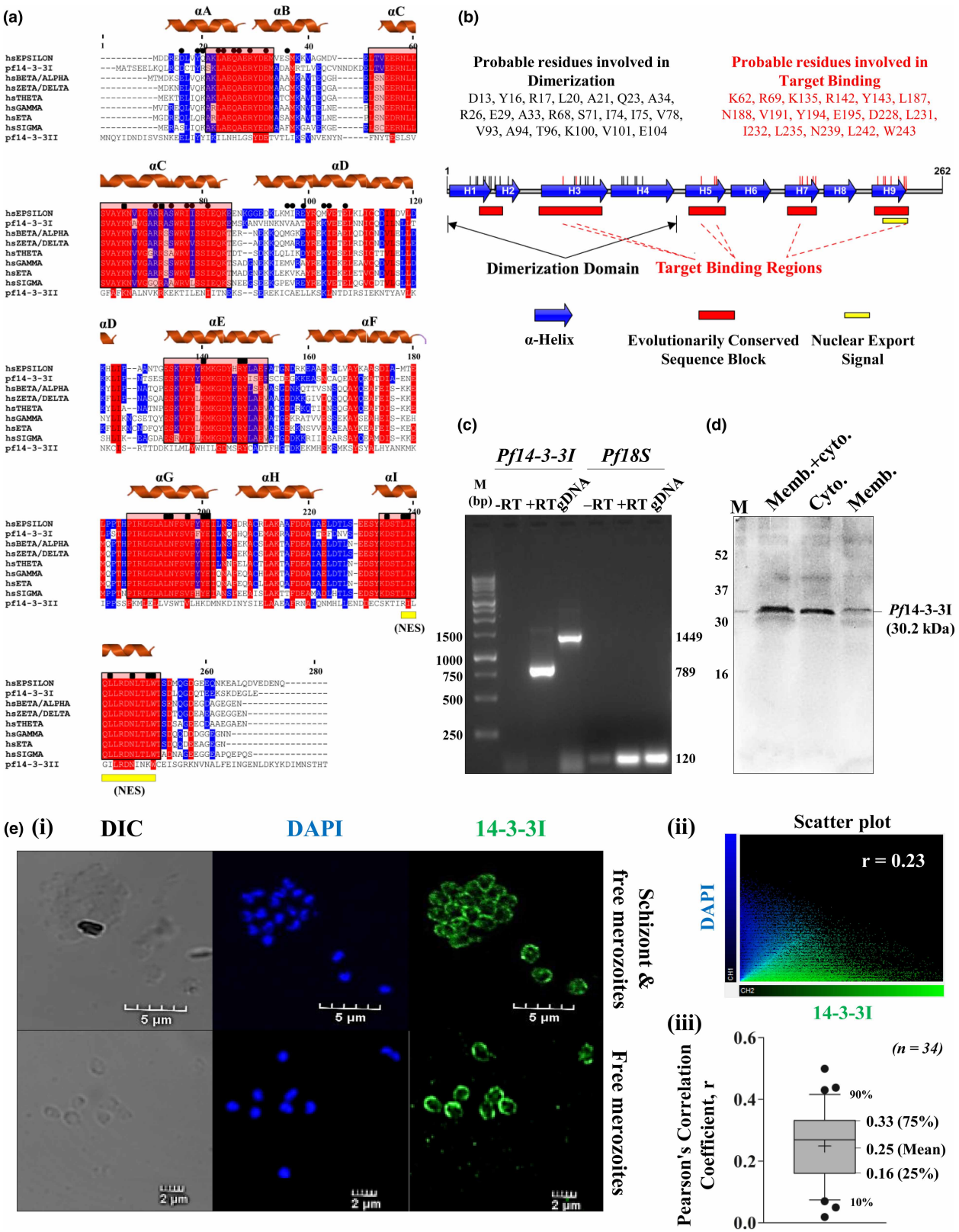

Figure 1. Comparative sequence analysis, protein architecture and identification of *P. falciparum* 14-3-3I. Part 1 of 2

(**a**) *MultAlin-based sequence alignment.* Multiple sequence alignment was performed to contextualize patterns of conservation and correlation in *Pf*14-3-3 protein sequences in light of well-studied orthologs in humans. Residues with high (>90%) and low (>50%, <90%) consensus values are

Figure 1. Comparative sequence analysis, protein architecture and identification of *P. falciparum* 14-3-3I. Part 2 of 2

shaded in red and blue, respectively. α-helices and NES are indicated. Five highly conserved sequence blocks are shown boxed and shaded red. Residues involved in dimerization (solid circles) and phosphopeptide binding (solid squares) are conserved in all 14-3-3 Isotypes, except *Pf*14-3-3II which appears to be the most divergent form. (**b**) *Overall Pf14-3-3I architecture.* Based on multiple sequence alignment, probable amino acid residues of *Pf*14-3-3I involved in dimerization and target binding are shown. *Pf*14-3-3I architecture was constructed by using Illustrator for Biological Sequences (IBS 1.0.3). (**c**) *Detection of Pf14-3-3 encoding cDNA. pf14-3-3I* transcript was amplified from cDNA prepared from schizonts, by using *pf14-3-3I* specific primer sets. Desired band size of 789 bp was seen, as compared with the band size of 1449 bp using gDNA as template. Amplification of *pf18S* was taken as positive control. The experiment was done twice. (**d**) *Western blot analysis of Pf14-3-3I.* In-house generated polyclonal sera raised in Balb/c mice against r14-3-3I was used to confirm the existence of native *Pf*14-3-3I protein in the parasite (schizonts) lysate. Desired protein band of 30.2 kDa was observed in both cytosolic and membrane fractions of the lysate. The experiment was done twice. (**e**) *Localization of Pf14-3-3.* Anti-r14-3-3I mice serum was used to probe localization of the protein in mature schizonts and free merozoites, by using confocal microscopy. *Pf*14-3-3 protein was found to be localized towards cell periphery (i). In the representative scatter plot (ii), green channel (*Pf*14-3-3I) is shown on the x-axis and blue channel (DAPI) is shown on the *y*-axis; and, $r = 0.25 \pm 0.12$ ($n = 34$) (iii). The experiment was done thrice. H1-H9: α-helices; M: DNA or protein marker; RT: Reverse Transcriptase; DIC: Differential Interference Contrast image.

stereochemical quality and accuracy of the homology model displayed 88.7% of amino acid residues lying in the most favored (*core*) regions, with 8.8%, 1.5%, and 1.1% residues in *additional allowed*, *generously allowed* and *disallowed regions* of Ramachandran plot, respectively (Supplementary Figure S1b). The comparable RMSD value and Ramachandran plot characteristics confirmed the reliability of the 3D-structural model of $Pf14\text{-}3\text{-}3I_{dimer}$ to be taken further for docking and simulation studies.

Unrooted phylogenetic relationship of *Pf*14-3-3 isoforms with their orthologs present across three major kingdoms of life: plantae, animalia and fungi showed that *Pf*14-3-3 isoforms have followed convergent evolutionary pathway with 14-3-3 proteins from plant *non-epsilon* group (Supplementary Figure S2a). Branches with green, red and blue squares represent 14-3-3 proteins from kingdom plantae, animalia and fungi, respectively. Detailed evolutionary relationship of *Pf*14-3-3 isoforms with their orthologs from plant *non-epsilon* group is shown in Supplementary Figure S2b.

Transcript encoding for *Pf*14-3-3I protein was amplified from cDNA prepared from schizonts, by using *pf14-3-3I* specific primers, as described in materials and methods section. Detection of desired DNA fragment of 789 bp indicated the presence of *Pf*14-3-3I encoding cDNA in the parasite, as compared with the band size of 1449 bp using gDNA as template (Figure 1c). Amplification of transcript encoding for 18s rRNA (120 bp) by using *pf18s* specific primers was taken as positive control. Furthermore, western blot analysis of native *Pf*14-3-3I protein in the parasite (schizonts) lysate, by using in-house generated polyclonal mice sera raised against r14-3-3I, confirmed the existence of *Pf*14-3-3I protein in the parasite (Figure 1d). Desired protein band of ∼30.2 kDa was observed in both Cytosolic (C) and Membrane (M) fractions of the parasite lysate. IFA in mature schizonts and free merozoites with the anti-r14-3-3I mice serum indicated localization of the protein towards cell periphery (Figure 1e (i)). In support of the confocal images, localization analysis is shown by a representative scatter plot (Figure 1e (ii)) and mean Pearson's correlation coefficient (r) (Figure 1e (iii)), as analyzed by using Olympus cellSens dimensions imaging software. Green intensity (*Pf*14-3-3I) is shown on the x-axis and blue intensity (DAPI) is shown on the y-axis; and, $r = 0.25 \pm 0.12$ ($n = 34$).

To *update* consensus 14-3-3 recognition motifs, literature search followed by mining of publically available databases was done to identify experimentally validated 14-3-3 interacting proteins present in prokaryotes and eukaryotes, and further collate details of 14-3-3 binding phosphoSer/Thr sites in the target proteins. In total, 323 Mode I sites from 243 target proteins, 81 Mode II sites from 77 target proteins and 9 Mode III sites from 9 target proteins were identified as gold-standard 14-3-3 binding *p*S/*p*T sites (Supplementary Table S1). Amino acid sequences of these 14-3-3 binding phosphopeptides were used to *update* consensus 14-3-3 binding motifs, as shown in Supplementary Figure S3a. Furthermore, key protein kinases of the parasite: *Pf*CDPK1, Protein Kinase G (*Pf*PKG), Protein Kinase A regulatory subunit ($PfPKA_R$) and Protein Kinase A catalytic subunit ($PfPKA_C$) were filtered out as putative binding partners of *Pf*14-3-3I, by combining global phosphoproteomic datasets of peptides enriched from schizont stage of *P. falciparum*, with 14-3-3 binding motifs search (Supplementary Figure S3b).

Biochemical Journal (2020) 477 2153–2177
https://doi.org/10.1042/BCJ20200145

Molecular Dynamics (MD) simulation reveals stable *Pf*14-3-3I$_{dimer}$/*p*CDPK1 complex formation

To probe the associated inter-molecular interactions that regulate *Pf*14-3-3I$_{dimer}$/*p*CDPK1 binding affinity, we performed MD simulation studies. A schematic representation of the interactions between *Pf*14-3-3I$_{dimer}$ and *p*CDPK1 is shown in Figure 2a. Peptide stretch, ^{61}KLGS^{64} of *p*CDPK1 was found to play a key role in mediating its interaction with *Pf*14-3-3I$_{dimer,}$ where a Hydrogen-bond was formed between S64 of *p*CDPK1 and K227 of *Pf*14-3-3I$_{dimer,}$ with a bond length of 2.92 Å. In addition to the Hydrogen-bond, inter-molecular association was further stabilized by hydrophobic interactions between S64 of *p*CDPK1 and Y226, Y555, E557, I597 constituting amphipathic groove of *Pf*14-3-3I$_{dimer}$. Furthermore, comprehensive analysis of the MD trajectories, i.e. Root Mean Square Deviation (RMSD), Radius of Gyration and variation in the Hydrogen-bond formation between *Pf*14-3-3I$_{dimer}$ and *p*CDPK1 were also reported as a function of simulation time (Figure 2a). The

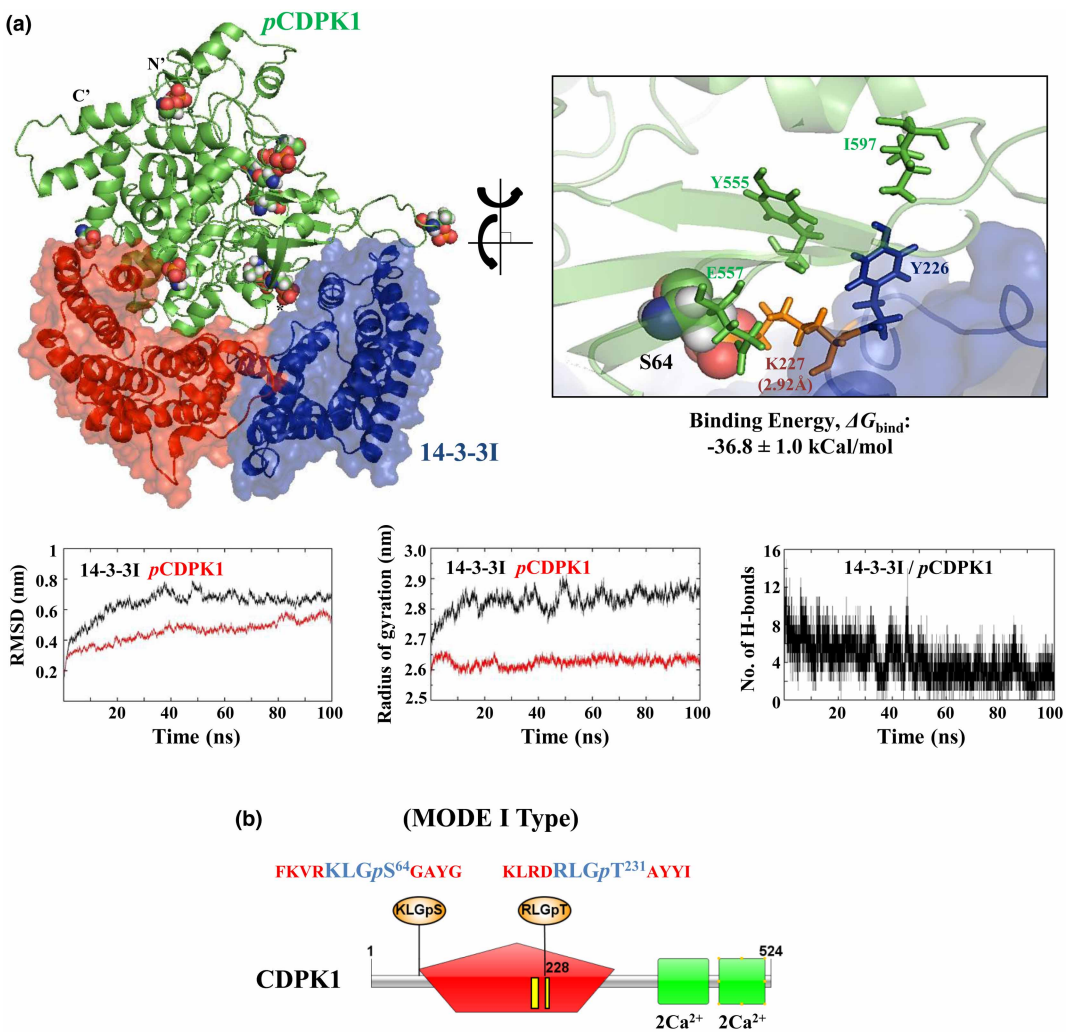

Figure 2. Molecular dynamics simulation of *Pf*14-3-3/*p*CDPK1 complex.

(**a**) *Schematic representation of the interactions between Pf14-3-3I$_{dimer}$ and pCDPK1.* Hydrogen-bond formation is shown between S64 of *p*CDPK1 and K227 of *Pf*14-3-3I$_{dimer}$, which has a bond length of 2.92 Å. The variation in RMSD and Radius of Gyration of *Pf*14-3-3I$_{dimer}$ and *p*CDPK1 is shown as a function of simulation time. The variation in number of inter-molecular Hydrogen-bond formation between *Pf*14-3-3I$_{dimer}$ and *p*CDPK1 is shown as a function of simulation time. (**b**) *Amino acid sequences of probable Pf14-3-3 binding phosphopeptides of PfCDPK1.* By combining global phosphoproteomic datasets of peptides enriched from schizont stage of *P. falciparum*, with 14-3-3 binding motifs search, peptide sequences of probable *Pf*14-3-3 binding regions of *Pf*CDPK1 were identified. RMSD: Root Mean Square Deviation.

Biochemical Journal (2020) 477 2153–2177
https://doi.org/10.1042/BCJ20200145

variation of RMSD and Radius of Gyration in *Pf*14-3-3I$_{dimer}$ and *p*CDPK1 clearly indicated a lesser stability and compactness in the former compared with the latter. Stability of the *Pf*14-3-3I$_{dimer}$/*p*CDPK1 complex was also confirmed by the extensive Hydrogen-bond formation between the two proteins, at different time intervals throughout the simulation run, and a negative binding free energy of −36.8 ± 1.0 kcal/mol, as obtained from MM/GBSA method. Movie S1 shows the interactions between *Pf*14-3-3$_{dimer}$ (blue) and *p*CDPK1 (grey).

Amino acid sequences of probable *Pf*14-3-3 binding phosphopeptides of *Pf*CDPK1 are shown in Figure 2b. These peptide stretches were identified by combining global phosphoproteomic datasets of peptides enriched from schizont stage of *P. falciparum*, with 14-3-3 binding motifs search.

*Pf*14-3-3I exhibits divergent binding affinities for CDPK1 and *p*CDPK1 *in vitro*

Purity level of r14-3-3I and rCDPK1 was checked by staining with Coomassie Brilliant Blue (Figure 3a (i) and (ii)). Phosphorylation status of rCDPK1 and r*p*CDPK1 was confirmed by in-gel fluorescence staining with Pro-Q Diamond phosphoamino acid stain (Figure 3a (iii)).

For ELISA based *Pf*14-3-3I/*Pf*CDPK1 PPI analysis, poly-L-Lysine treated 96-welled microtitre plate was coated with the bait protein, rCDPK1 (or r*p*CDPK1), followed by addition of increasing concentrations of the prey protein, r14-3-3I (or GST, as negative control). The interaction analysis was done by using monoclonal antibody against GST protein. Concentration dependent binding between rCDPK1 (or r*p*CDPK1) and r14-3-3I was observed (Figure 3b). Furthermore, PPI analysis by ELISA indicated that phosphorylation status of *Pf*CDPK1 dictates its interaction with r14-3-3I. No significant absorbance ($OD_{490\ nm}$) was observed for interaction of rCDPK1 (or, r*p*CDPK1) with GST alone. To quantitate the interaction between rCDPK1 (or r*p*CDPK1) and r14-3-3I, SPR analysis was performed by using AutoLab Esprit SPR. r14-3-3I was immobilized at an average density of 4.3 ng per 1 mm^2 of the sensor chip surface. Once immobilized, r14-3-3I demonstrated good stability throughout the experiment. Interaction analysis was done by injecting serial dilutions of either rCDPK1 or r*p*CDPK1, ranging from 100 nM to 1 μM, over the r14-3-3I-immobilized sensor chip surface, followed by comparing their respective kinetics and binding affinities at RT. With increase in mass concentration of rCDPK1 and r*p*CDPK1, gradual increase in sensor signal was observed, which linearly correlated with corresponding change in refractive index of the medium immediately adjacent to the SPR sensing surface. Concentration dependent real-time sensorgrams alongwith K_D values of the interactions are shown in Figure 3c. rCDPK1 and r*p*CDPK1 showed differential binding affinities for r14-3-3I, with K_D values of 0.67 ± 0.0036 μM and 1.35 ± 0.0083 μM, respectively. To provide mechanistic insight into the role of *Pf*14-3-3 in regulating *Pf*CDPK1 activity, we tested kinase activity of rCDPK1 *in vitro*, in the presence of r14-3-3. However, we observed only marginal increment in the phosphorylation status of casein, and no significant increase in auto-phosphorylation status of *Pf*CDPK1, as confirmed by in-gel staining of the reaction mixtures with Pro-Q Diamond phosphoamino acid stain (Figure 3d and Supplementary Figure S4).

IFA was performed on synchronized *P. falciparum* 3D7 culture to check for co-localization of 14-3-3I and CDPK1, by probing mature stages of the parasite with anti-*Pf*14-3-3I mouse-serum and anti-*Pf*CDPK1 rabbit-serum. 14-3-3I protein was found to co-localize very nicely with CDPK1 protein towards cell periphery, in mature schizonts and free merozoites (Figure 3e (i)). In support of the confocal images, co-localization analysis is shown by a representative scatter plot (Figure 3e (ii)) and mean Pearson's correlation coefficient (r) (Figure 3e (ii)), as analyzed by using Olympus cellSens dimensions imaging software. Green intensity (*Pf*14-3-3I) is shown on the x-axis and red intensity (*Pf*CDPK1) is shown on the y-axis; and, $r = 0.79 \pm 0.04$ ($n = 34$). Yellow dots on the scatter plot show the co-localization of *Pf*14-3-3I and *Pf*CDPK1.

We utilized two different phosphopeptides: Mode I (ARSH*p*SYPA or *peptide 1*) and Mode II (RLYH*p*SLPA or *peptide 2*) (*pS*: phosphoserine) to inhibit *Pf*14-3-3/*Pf*CDPK1 interaction [87–92], as mentioned in materials and methods section. These phosphopeptides were identified by Rittinger et al. [29] from oriented peptide library screening, and are recognized by all mammalian and *S. cerevisiae* 14-3-3 isotypes.

MD simulation reveals stable *Pf*14-3-3I$_{dimer}$/peptides (1 or 2) complex formation

Molecular interactions between *Pf*14-3-3I$_{dimer}$ and phosphopeptides (1 or 2) were studied by performing 20 ns MD simulations (Figure 4a). Peptide 1 was found to bind in the amphipathic groove of the receptor protein, *Pf*14-3-3I$_{dimer}$. Here, three Hydrogen-bonds were formed between phosphoSer of peptide 1 and K306, K379, S302 constituting amphipathic groove of *Pf*14-3-3I$_{dimer}$, in addition to hydrophobic interactions that further

Biochemical Journal (2020) **477** 2153–2177
https://doi.org/10.1042/BCJ20200145

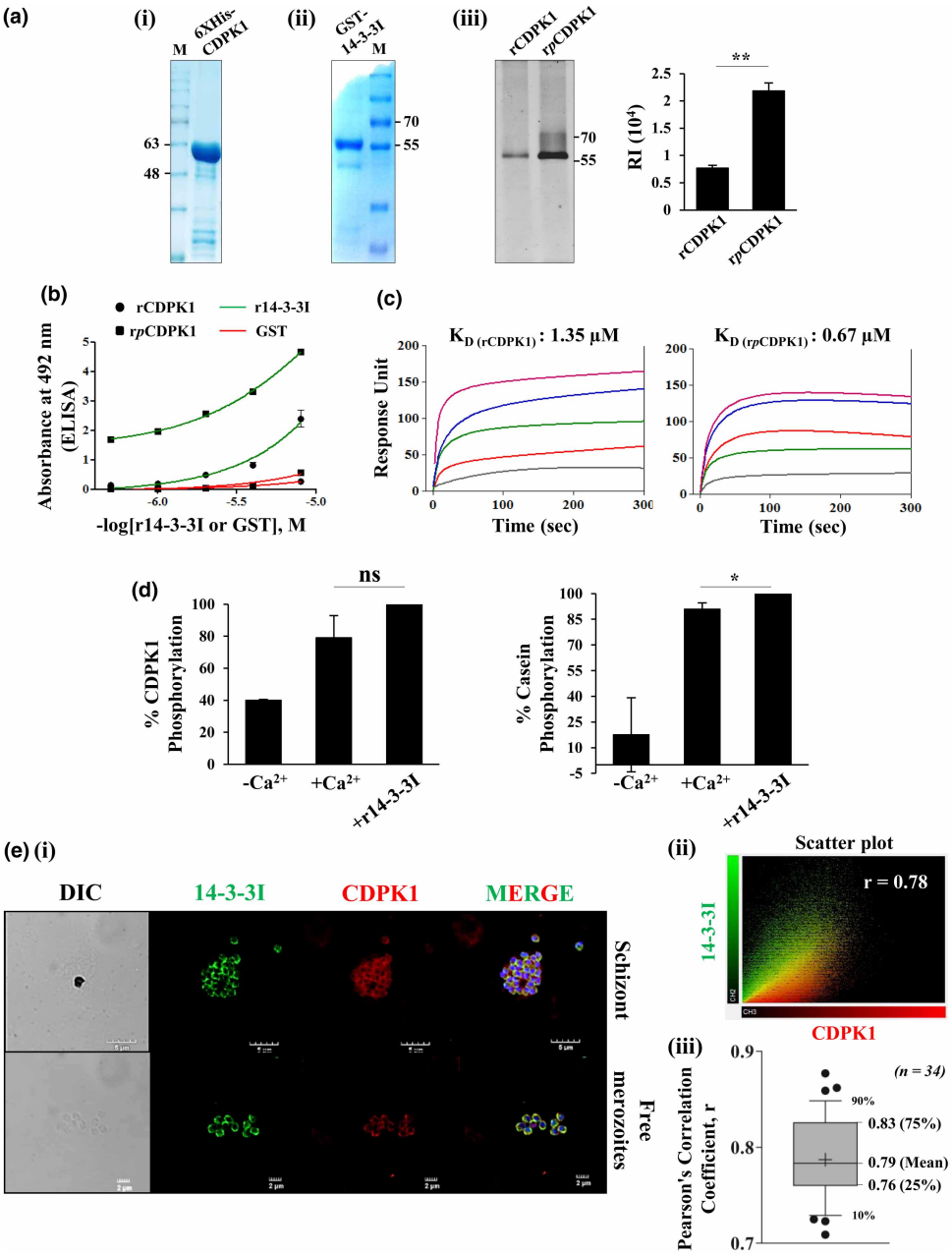

Figure 3. *Pf*14-3-3I interacts with *Pf*CDPK1 *in vitro*. Part 1 of 2

(**a**) Coomassie-stained gels showing the level of purity of rCDPK1 (**i**) and r14-3-3I (**ii**) used for all *in vitro* experiments. Phosphorylation status of rCDPK1 and *rp*CDPK1, as confirmed by in-gel fluorescence staining with Pro-Q Diamond phosphoamino acid stain (**iii**). (**b**) *ELISA.* For *Pf*14-3-3I/*Pf*CDPK1 interaction analysis, a kinase reaction was set up with rCDPK1 (100 ng/µl), in the absence and presence of Ca^{2+}-ions for conditions requiring rCDPK1 and *rp*CDPK1, respectively. rCDPK1 or *rp*CDPK1 (200 ng) was coated onto Poly-L-Lysine coated microtitre plates, followed by incubation with 0.5 to 8 µM concentrations of r14-3-3I (green) or GST (red) as negative control. Interaction analysis was done by using monoclonal antibody against GST protein. r14-3-3 was found to interact with rCDPK1 in a phosphorylation dependent manner. No significant absorbance ($OD_{490\ nm}$) was observed for interaction of rCDPK1 (or, rpCDPK1) with GST alone. The experiment was done twice in triplicates. (**c**) *Concentration dependent real-time sensograms for SPR based biomolecular interaction analysis.* ELISA based *Pf*14-3-3I/*Pf*CDPK1 interaction was further confirmed with AutoLab Esprit SPR. rCDPK1 and *rp*CDPK1 showed differential binding affinities for r14-3-3I, with K_D values varying from 0.67 ± 0.0036 µM and 1.35 ± 0.0083 µM, respectively. The experiment was done twice. (**d**) *r14-3-3I confers only marginal increase in the functional activity of rCDPK1 in vitro.* Estimates of

Figure 3. *Pf*14-3-3I interacts with *Pf*CDPK1 *in vitro*. Part 2 of 2

band intensities of *Pf*CDPK1 and casein from phosphostained gel images are shown in the form of bar graphs. The experiment was done twice. (**e**) *Co-localization of Pf14-3-3I and PfCDPK1. Pf*14-3-3I was found to co-localize very nicely with *Pf*CDPK1 towards cell periphery in mature schizonts and free merozoites (i). In the representative scatter plot (ii), green channel (*Pf*14-3-3I) is shown on the x-axis and red channel (*Pf*CDPK1) is shown on the y-axis; and, $r = 0.79 \pm 0.04$ ($n = 34$) (iii). Yellow dots on the scatter plot show the co-localization of *Pf*14-3-3I and *Pf*CDPK1. The experiment was done thrice. RI: Relative Intensity; K_D: Affinity constant; DIC: Differential Interference Contrast image, ns: not significant.

stabilized the association. Similarly, phosphoSer of peptide 2 formed a Hydrogen-bond with N188 of *Pf*14-3-3I$_{dimer}$, along with stabilizing hydrophobic interactions. A comparative study using time-dependent variations in RMSD and Radius of Gyration, however, revealed that *Pf*14-3-3I$_{dimer}$/peptide 2 complex was more stable and slightly more compact compared with *Pf*14-3-3I$_{dimer}$/peptide 1 complex. The observation was supported by the higher number of inter-molecular Hydrogen-bonds that are formed between *Pf*14-3-3I$_{dimer}$ and peptide 2, as compared with peptide 1. This also accounts for the higher negative binding free energy observed for *Pf*14-3-3I$_{dimer}$/peptide 2 complex (-67.2 ± 0.1 kcal/mol) relative to *Pf*14-3-3I$_{dimer}$/peptide 1 complex (-41.8 ± 1.0 kcal/mol). Supplementary Movies S2 and S3 show the interactions of *Pf*14-3-3$_{dimer}$ (blue) with peptides 1 and 2 (yellow), respectively.

Phosphopeptides 1 and 2 interact with *Pf*14-3-3I *in vitro*

After affirming the interaction of *Pf*14-3-3I$_{dimer}$ with phosphopeptides 1 and 2 through MD simulation studies, we further sought to establish the knowledge of binding modes of complexation, by employing ITC. This was achieved by determining binding affinity constant (K_a), and thermodynamic parameters associated with the interaction, like change in enthalpy (ΔH), binding free energy (ΔG) and entropy (ΔS). The representative binding isotherms resulting from titration of peptides (1 or 2) with r14-3-3I are shown in Figure 4b. Binding isotherms for peptide 1 and 2 were sigmoidal in nature ending near zero baselines, indicating saturation of r14-3-3's binding sites. In Figure 4b, solid line shows the best fit of the non-linear experimental data, and the model reproduces experimental data fairly well. On the basis of K_a values, binding strength was found to be higher in case of r14-3-3I/peptide 1 complex (K_a: $1.7 \times 10^6 \pm 6.8 \times 10^5$ M^{-1}) than that of r14-3-3I/peptide 2 (K_a: $8.3 \times 10^5 \pm 2.67 \times 10^5$ M^{-1}). For peptides 1 and 2, binding stoichiometry (N) was found to be 0.3–0.4 and ∼1.0, respectively. Moreover, it was observed that the binding of peptide 1 with r14-3-3I protein was enthalpically favorable ($\Delta H = -11.34 \pm 4.27$ kcal/mol), whereas entropically unfavorable [$T\Delta S = -2.8$ kcal/mol (±15–20%)], resulting in strong binding free energy [$\Delta G = -8.5$ kcal/mol (±15–20%)]. Higher negative ΔH value indicates the ability of peptide 1 to form a strong network of H-bonds and Van Der Waals interactions with *Pf*14-3-3I protein. The associated unfavorable ΔS value may be the result of loss of conformational freedom upon binding with *Pf*14-3-3I. For r14-3-3I/peptide 2 complex, the interaction was enthalpically as well as entropically driven [$\Delta H = -1.52 \pm 0.096$ kcal/mol, $T\Delta S = 6.5$ kcal/mol (±15–20%) and $\Delta G = -8.0$ kcal/mol (±15–20%)]. Higher positive ΔS value suggests contribution from *solvation entropy*, which results from the loss of water molecules from the binding surfaces of interacting partners when they come close together to form a complex [93]. And, small negative ΔH value indicates smaller number of H-bonds contributing to the formation of *Pf*14-3-3I/peptide 2 complex.

Phosphopeptides 1 and 2 antagonize *Pf*14-3-3I/*Pf*CDPK1 interaction

ELISA based *Pf*14-3-3I/*Pf*CDPK1 PPI analysis was performed in the presence of varying concentrations of phosphopeptides (1 or 2). Concentration dependent r14-3-3I/r*p*CDPK1 interaction inhibition was observed (Figure 5a). To further confirm ELISA results, western blot based GST pull-down assay was performed in which r14-3-3I (or GST, as negative control) was coupled with Glutathione Sepharose® 4B beads, followed by binding with rCDPK1 or r*p*CDPK1 to form bead-bound protein complexes, in the absence and presence of 10 μM concentration of the peptides. Immunoblotting with HRP-conjugated anti-His antibody indicated that phosphorylation status of *Pf*CDPK1 dictates its interaction with *Pf*14-3-3I, as confirmed by ELISA (Figure 5b). Moreover, interaction inhibition was readily observed in the presence of peptides (1 or 2). The same blot stripped and re-probed with HRP-conjugated anti-GST antibody confirmed equal coupling of r14-3-3I (or GST) with the beads in all binding reactions.

Biochemical Journal (2020) **477** 2153–2177
https://doi.org/10.1042/BCJ20200145

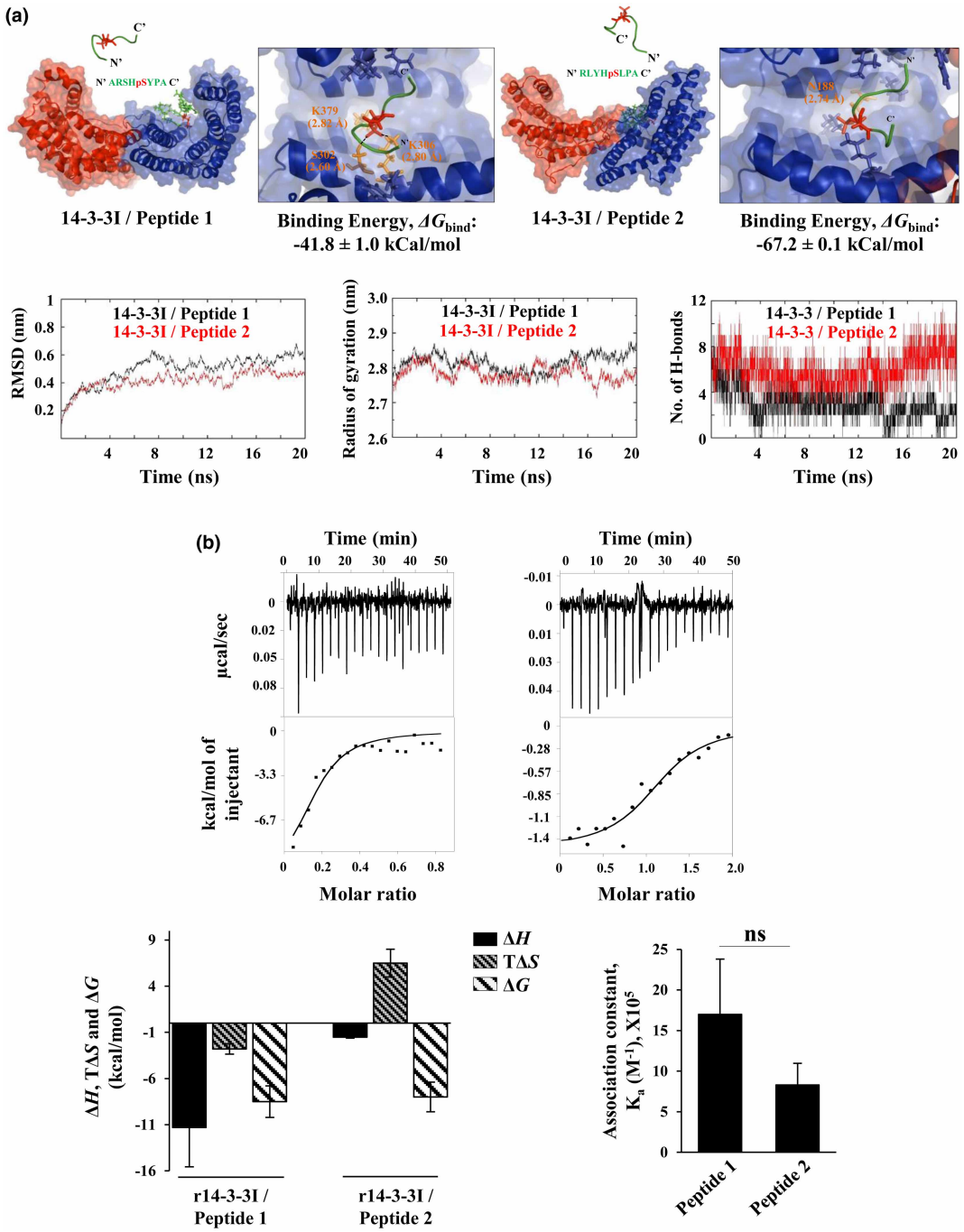

Figure 4. Phosphopeptides 1 and 2 interact with *Pf*14-3-3I. Part 1 of 2

(**a**) *Schematic representation of the interactions between Pf14-3-3I$_{dimer}$ and phosphopeptides 1 (left)* and *2 (right).* The Hydrogen-bonds formed between phosphoSer of peptide 1 and K306, K379, S302 of *Pf*14-3-3I$_{dimer}$ (left); and, phosphoSer of peptide 2 and N188 of *Pf*14-3-3I$_{dimer}$ (right). Also shown, the variation in RMSD and Radius of Gyration of *Pf*14-3-3I$_{dimer}$ when it interacts with peptides (1 or 2); and, the variation in number of inter-molecular Hydrogen-bonds formed between *Pf*14-3-3I$_{dimer}$ and peptides (1 or 2), as a function of simulation time. (**b**) *Representative binding isotherms resulting from titrations of r14-3-3I with phosphopeptides (1 or 2).* ITC was employed to determine kinetic parameters of complexation between r14-3-3I (10 µM) and peptide 1 (40 µM) or 2 (100 µM), by using MicroCal iTC200. On the basis of K_a values, binding strength was found to be higher in case of *Pf*14-3-3I/peptide 1 (K_a: $1.7 \times 10^6 \pm 6.8 \times 10^5$ M^{-1}) than in case of *Pf*14-3-3I/peptide 2 (K_a: $8.3 \times 10^5 \pm 2.67 \times 10^5$ M^{-1}) interaction. The binding of peptide 1 with r14-3-3I was enthalpically favorable whereas

Figure 4. Phosphopeptides 1 and 2 interact with *Pf*14-3-3I. Part 2 of 2

entropically unfavorable, resulting in strong binding free energy. For *Pf*14-3-3I/peptide 2 complex, the interaction was enthalpically as well as entropically driven. Experimental data is represented as the amount of heat released per second (μcal/sec; corrected for heat of dilution of the ligand) following each injection of the ligand (peptide) into the receptor protein (r14-3-3I), as a function of time (min.). The data were fitted by using single-site binding model. Solid line represents the best fit of the non-linear experimental data. The experiment was done twice. RMSD: Root Mean Square Deviation; ΔH: change in Enthalpy; ΔS: change in Entropy; ΔG: change in Gibbs free energy; T: Temperature, ns: not significant.

Phosphopeptides 1 and 2 with propensity to bind *Pf*14-3-3I and inhibit *Pf*14-3-3I/*Pf*CDPK1 interaction, were further subjected to *P. falciparum* invasion inhibition *in vitro*. Towards this, mature (punctated) schizonts were allowed to burst and invade into erythrocytes, in the presence of 12.5 μM concentration of the peptides. Untreated parasites served as control and percentage of parasite invasion was evaluated by flow cytometry, as described in materials and methods section. Peptides 1 and 2 showed significant inhibition in progression of schizonts to ring stage of the parasite (Figure 5c (i)). Giemsa stained microscopic images of mature schizonts incubated with peptides 1 and 2 are shown in Figure 5c (ii). Control parasites were healthy, producing healthy rings at 22 h post-incubation. Whereas, upon treatment with the peptides, merozoite invasion inhibition was observed with significant alteration in parasite morphology. Here, relatively less number of ring parasitized erythrocytes were observed, alongwith the accumulation of pyknotic forms of the parasite.

Discussion

There are only a few evidences in literature which support the existence of 14-3-3 protein in Plasmodium species. *14-3-3* gene in *P. falciparum* and *P. knowlesi* was first identified by Al-Khedery et al. [94], who reported that *pk14-3-3* transcript begins to be expressed in the ring-stage, predominates in young trophozoites, and thereafter declines, during asexual intra-erythrocytic proliferative stages of the parasite. Also, antiserum raised against recombinant *Pk*14-3-3 was able to cross-react with *Pf*14-3-3. Later, Lalle et al. [95] showed that in *P. berghei* parasitized erythrocytes, the host junctional complex protein, demantin, is repositioned to the parasite where it interacts with *Pb*14-3-3 in a phosphorylation dependent manner, thus influencing remodeling of the erythrocytic skeleton. Furthermore, Dastidar et al. [96] identified *Pf*14-3-3 as a novel member of *P. falciparum* histone phosphosite binding protein repertoire, isolated from asexual blood stages of the parasite.

Two 14-3-3 isoforms are annotated in *P. falciparum* by PlasmoDB database curators: *Pf*14-3-3I and *Pf*14-3-3II. Upon their comparative sequence analysis with structurally and functionally characterized orthologs from humans, we reported patterns of sequence and structural conservation in *Pf*14-3-3I protein sequence, particularly encompassing amino acid residues at the dimerization interface and those involved in phosphopeptide binding. Concomitantly, our phylogenetic analysis showed that despite having evolved separately since the early eukaryotes, *Pf*14-3-3I has followed convergent evolution with plant *non-epsilon* group. In plants, the *epsilon* group of 14-3-3 proteins is considered as *ancestral* and destined to fulfil fundamental cellular functions; whereas, the *non-epsilon* group evolved later and members of this group might be related to organism *specific* functions [97]. We further confirmed the presence of 14-3-3 in the malaria parasite by employing various molecular biology techniques. Real-time PCR indicated the presence of transcript encoding for *Pf*14-3-3I protein. Western blot analysis using in-house generated polyclonal sera raised in mice against recombinant *Pf*14-3-3I protein indicated the presence of full length protein in the parasite. Furthermore, confocal microscopic imaging in mature schizonts and free merozoites indicated that *Pf*14-3-3I protein localizes towards the cell periphery.

In metazoans, kinases have been reported to be functionally modulated as a consequence of their interaction with 14-3-3 proteins. In this regard, first report came from Aitken et al. (1990, 1992) who identified 14-3-3 as one of the potent *inhibitors* of Ca^{2+}-dependent Protein Kinase C (PKC) in sheep brain, where it could *inhibit* phosphorylation activity of the kinase over a wide range of Ca^{2+}-ion concentrations [98–100]. In the concurrent year, Robinson et al. [101] investigated the mechanism of action of individual 14-3-3 isoforms in the inhibition of PKC. In the same line, Wheeler-Jones et al. [102] used synthetic peptides derived from conserved sequences of 14-3-3 that resemble pseudo-substrate regions of PKC and annexins, and suggested that 14-3-3 isoforms play a physiological role as inhibitors of PKC activity in human platelets, but are unlikely to be involved in controlling association of PKC with the membrane. Furthermore, Hausser et al. [103] identified 14-3-3*tau* as a

Biochemical Journal (2020) **477** 2153–2177
https://doi.org/10.1042/BCJ20200145

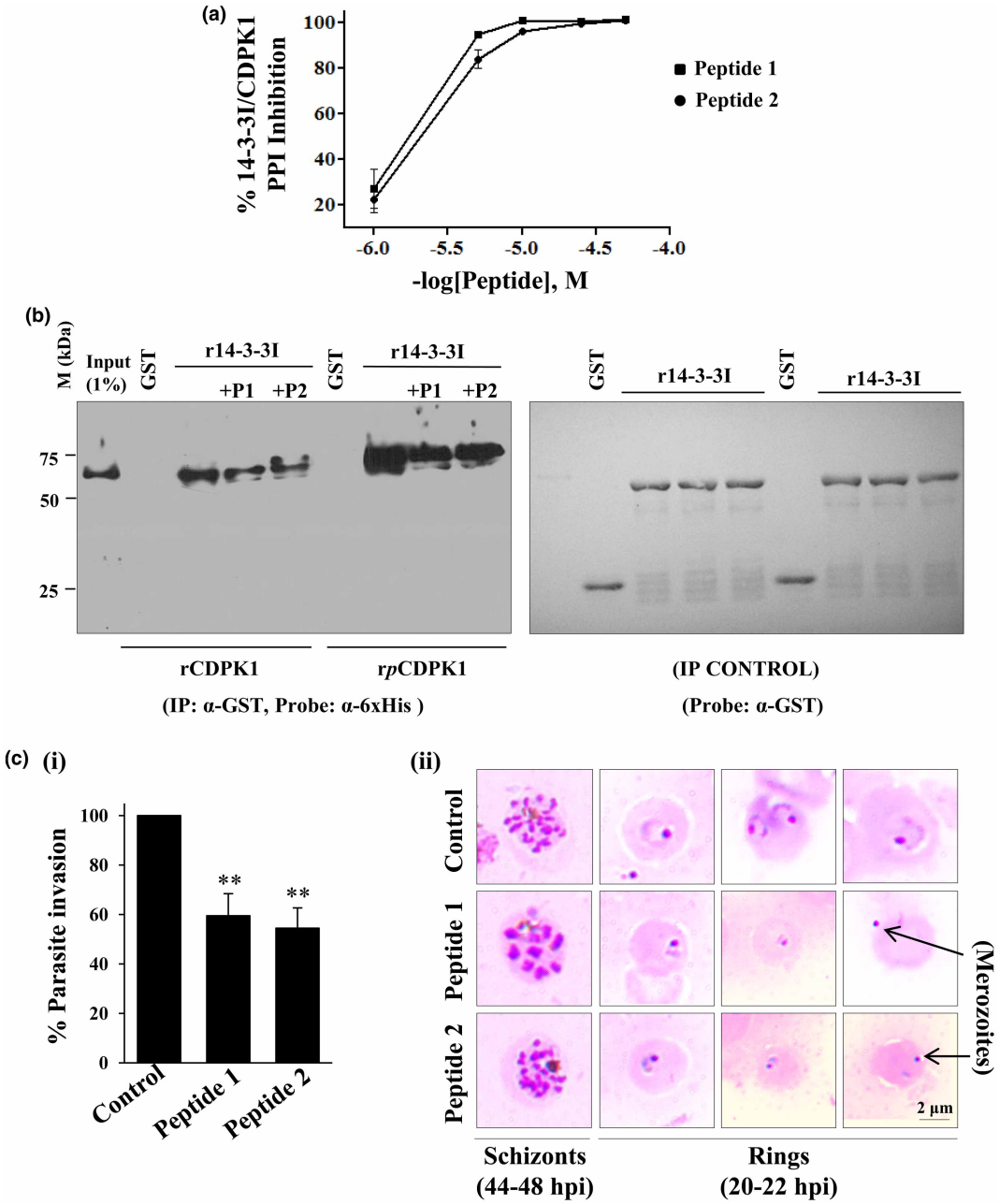

Figure 5. Phosphopeptides 1 and 2 antagonize *Pf*14-3-3I/*Pf*CDPK1 interaction. Part 1 of 2

(**a**) *ELISA*. Concentration dependent inhibition in binding of *rp*CDPK1 with r14-3-3I was observed in the presence of phosphopeptides (1 or 2; 1 μM to 50 μM). Interaction analysis was done by using monoclonal antibody against GST protein. The experiment was done twice in triplicates. (**b**) *GST-based pull-down assay.* ELISA based *Pf*14-3-3I/*Pf*CDPK1 interaction inhibition was further confirmed by western blot based GST pull-down assay in which Glutathione Sepharose® 4B beads was coupled with r14-3-3I (10 μg), followed by incubation with rCDPK1 or *rp*CDPK1 (10 μg), in the absence and presence of peptides (1 or 2; 10 μM). Immunoblotting with HRP-conjugated anti-His antibody indicated that phosphorylation status of *Pf*CDPK1 dictates its interaction with *Pf*14-3-3I. Moreover, interaction inhibition was readily observed in the presence of both peptides. Same blot stripped and re-probed with HRP-conjugated anti-GST antibody confirmed equal coupling of r14-3-3I (or GST) with the beads in all binding reactions. The blots shown are representative of two independent experiments. (**c**) *Parasite invasion assay.* Mature schizonts were allowed to invade into erythrocytes in the presence of peptides (1 or 2) (12.5 μM). % parasite invasion was calculated by FACS using BD LSRFortessa™ cell analyzer. Untreated parasites served as control. Both peptides significantly inhibited progression of schizonts to ring stage **(i)**. Control parasites were healthy, producing healthy

Figure 5. Phosphopeptides 1 and 2 antagonize *Pf*14-3-3I/*Pf*CDPK1 interaction. Part 2 of 2

rings at 22 h post-incubation. Whereas, upon treatment with the peptides, merozoite invasion inhibition was observed with significant alteration in parasite morphology **(ii)**. Here, relatively less number of ring parasitized erythrocytes were observed, alongwith the accumulation of pyknotic forms of the parasite. The experiment was done twice in triplicates. M: Protein marker; P1: Phosphopeptide 1; P2: Phosphopeptide 2.

negative regulator of PKCμ, in which 14-3-3*tau* was reported to inhibit PKCμ kinase activity both *in vitro* and in intact T-cells. In contradiction to these studies, Isobe et al. [104] showed that a member of the 14-3-3 family, termed 'Exo1', *activates* PKC by two-fold. This finding raised the possibility that the ability of Exo1 to reactivate Ca^{2+}-dependent exocytosis might be based on its stimulatory effect on PKC activity. In the same line, Tanji et al. [105] also identified 14-3-3 isoforms as *activators* of PKC in bovine forebrain. Unlike previously reported, the activation of PKC by 14-3-3 was found to be independent of phosphatidylserine and Ca^{2+}-ions and, as such, the study provided an alternative mechanism for the activation of PKC that obviates its translocation to membranes. Later, Acs et al. [106] reported differential *activation* of various PKC isoforms, especially PKC epsilon, by 14-3-3 zeta protein in humans.

In addition to PKC, 14-3-3 proteins have also been reported to bind and modulate functional activity of other kinases. For instance, Fantl et al. [107] reported that 14-3-3 isoforms bind to and *enhance* Ser/Thr kinase activity of Raf-1, a key mediator of mitogenesis and differentiation, thus promoting Raf-1 dependent oocyte maturation. Next, Takihara et al. [108] reported that overexpression of 14-3-3β stimulates cellular proliferation and oncogenic transformation of mouse derived fibroblast cell line, by interacting with and *enhancing* Raf-1 activation and resultant augmentation of signaling in Mitogen-Activated Protein Kinase (MAPK) cascade. In the subsequent year, Rothblum-Oviatt et al. [109] reported that 14-3-3 proteins function as *positive regulators* of human Wee1, a tyrosine-specific protein kinase that phosphorylates mitotic inducer Cell division control 2 (Cdc2), and induce Wee1 mediated G2 cell cycle delay. Later, Kim et al. [110] reported that 14-3-3 interacts with and *enhance* functional activity of Dual-specificity tyrosine(Y) regulated kinase 1A (DYRK1A), a serine/threonine protein kinase implicated in mental retardation resulting from Down syndrome. Furthermore, Fischer et al. [111] demonstrated that 14-3-3 proteins associate with and *activate* serine/threonine-specific RAF isoforms (A, B and C) in a isoform-specific manner, thus further elucidating complex mechanism of RAF activation. More recently, Yuasa et al. [112] demonstrated that Death-Associated Protein Kinase 2 (DAPK2; a Ca^{2+}/calmodulin-regulated serine/threonine kinase)-induced apoptosis is *negatively regulated* by its interaction with 14-3-3 proteins.

In the current study, we report that *Pf*14-3-3 isoform I interacts with *Pf*CDPK1, a highly expressed protein in the malaria parasite, which plays key role in multitude of essential cellular processes, including parasite invasion and egress during intra-erythrocytic proliferative stages of the parasite. Preliminary structural modeling and MD simulation studies of *Pf*14-3-3I_{dimer}/*p*CDPK1 complex indicated that *Pf*CDPK1 binds to the amphipathic groove of *Pf*14-3-3I_{dimer} in a thermodynamically stable manner. The interaction is largely driven by charged residues present at the interface of the two proteins, and hydrophobic interactions further stabilize the association. Variation of RMSD and Radius of Gyration indicated conformational fluctuations in *Pf*14-3-3I_{dimer} upon binding to *p*CDPK1, which may assist in forming a stable complex via induced-fit mechanism [113,114]. The simulation results were confirmed experimentally by combining various biochemical and biophysical approaches. ELISA based PPI analysis indicated that *Pf*14-3-3I interacts with *Pf*CDPK1 in a phosphorylation dependent manner. The associated binding strength of the interaction was subsequently quantified by SPR, which indicated that *Pf*14-3-3I has approximately two fold higher affinity towards *p*CDPK1 than for CDPK1. In a related unpublished study by our group, the phosphorylation dependent interaction of *Pf*14-3-3I with *Pf*CDPK1 was validated in merozoites, wherein, by pulling down *Pf*14-3-3I, *Pf*CDPK1 was detected in a Ca^{2+}-dependent manner [115]. Our finding overlap with the conception that phosphorylation of target protein is a prerequisite for its interaction with 14-3-3. SPR sensograms suggested specificity of *Pf*CDPK1 towards *Pf*14-3-3I cavity(ies) in terms of shape complementarity and chemical functionality. Kinase assay in the presence of r14-3-3I suggested that *Pf*14-3-3 binding is not required in regulating *Pf*CDPK1 enzymatic activity *in vitro*. Furthermore, confocal microscopic imaging in mature schizonts and free merozoites indicated that *Pf*14-3-3I co-localizes well with *Pf*CDPK1, towards the cell periphery.

Earlier reports suggest that synthetic peptides containing phosphorylated 14-3-3 binding motifs can efficiently inhibit the association of 14-3-3 proteins with their interacting partners, by typically binding to their conserved amphipathic grooves. The first report utilizing peptides as 14-3-3 binding high-affinity *antagonists*

Biochemical Journal (2020) 477 2153–2177
https://doi.org/10.1042/BCJ20200145

came from Wang et al. [87], who identified unphosphorylated peptide (PHCVPRDLSWLDLEANMCLP), termed R18, by screening phage display libraries. The peptide bound to the amphipathic groove of 14-3-3, without isoform selectivity. R18 efficiently blocked the interaction of 14-3-3 with Raf-1 kinase, thereby effectively abolishing the protective role of 14-3-3 against phosphatase-induced inactivation of Raf-1, and virulence factor exoenzymeS (ExoS) of the pathogenic bacterium *Pseudomonas aeruginosa* [87,88]. To further enhance R18 activity in cells, a dimeric R18 sequence, termed *difopein* (*di*meric *fo*urteen-three-three *pe*ptide *in*hibitor), was used to dissect the physiological role of 14-3-3/client-protein interaction, and served as a basis for targeting pro-survival function of 14-3-3, as a potential anticancer strategy [89]. Thereafter, other peptide-based inhibitors have been developed, such as macrocyclic cross-linked peptide synthesized by Glas et al. [90] and Cromm et al. [91] that inhibit the interaction between human 14-3-3 and ExoS. The so-called ESp peptide (^{420}QGLLDALDLAS^{430}) which is a 14-3-3 binding motif of ExoS, was used as a starting point for designing macrocyclic PPI inhibitor with different cross-link architectures. Later, Milroy LG *et al.* (2015) synthesized Tau peptide *hybrids* to inhibit 14-3-3/Tau interaction, a potential drug target for the treatment of Alzheimer's disease [92]. The peptides were designed with an extended hydrophobic area at the C-terminus that targeted the highly conserved pocket within the amphipathic groove of 14-3-3.

Based on the literature review and owing to the fact that well characterized 14-3-3 recognition motifs (Mode I, II and III) and other naturally occurring 14-3-3-binding peptides can be utilized as 14-3-3/client-protein PPI *antagonists*, we utilized two different phosphopeptides: Mode I (ARSH*pS*YPA or *peptide 1*) and Mode II (RLYH*pS*LPA or *peptide 2*) (*pS*: phosphoserine) to inhibit *Pf*14-3-3/*Pf*CDPK1 interaction. These phosphopeptides were identified by Rittinger et al. [29] from oriented peptide library screening, and are recognized by all mammalian and *S. cerevisiae* 14-3-3 isotypes. Preliminary structural modeling and molecular dynamics simulation studies of *Pf*14-3-3I$_{dimer}$/peptides (1 or 2) complexes indicated that the peptides bind to the amphipathic groove of *Pf*14-3-3I$_{dimer}$ in a thermodynamically stable manner. The interaction is largely driven by Hydrogen-bonds between phosphoSer of the peptide ligands and amino acid residues constituting the conserved amphipathic groove of the receptor protein, and the association is further stabilized by hydrophobic interactions. The stable complex formation between *Pf*14-3-3I$_{dimer}$ and phosphopeptides (1 or 2) suggests effectiveness of the peptides as potential inhibitors of *Pf*14-3-3I$_{dimer}$ mediated interactions. The simulation results were experimentally confirmed by ITC with r14-3-3I and peptides synthesized *de novo*. Peptide 1 showed higher binding affinity for r14-3-3I than peptide 2. Much stronger ΔH value for peptide 1 indicates its ability to form a strong network of Hydrogen-bonds and Van Der Waals interactions with *Pf*14-3-3I protein. The associated unfavorable entropy may be the result of loss of conformational freedom upon *Pf*14-3-3I/peptide 1 complex formation. In case of peptide 2, interactions are strongly dominated by favorable entropy, with a slight contribution from enthalpy. Positive entropy suggests important contribution from *solvation entropy*, which results from the loss of water molecules from the binding surfaces of interacting partners when they come close together to form a complex [93]. Small negative ΔH value indicates smaller number of H-bonding interactions contributing to the formation of *Pf*14-3-3I/peptide 2 complex. Moreover, for peptide 1, binding stoichiometry (N) of 0.3-0.4 indicates binding of one peptide molecule per two or three molecules of r14-3-3I, which may be due to some additional non-specific interactions, apart from specific binding. Interaction with peptide 2 resulted in N ~ 1.0, which indicates binding of one peptide molecule per molecule of r14-3-3I. Furthermore, both peptides 1 and 2 efficiently blocked the interaction of *Pf*14-3-3I with *Pf*CDPK1, as confirmed by ELISA and pull-down experiments with recombinantly purified proteins. To dissect the physiological role of *Pf*14-3-3I/*Pf*CDPK1 interaction, mature *P. falciparum* schizonts were allowed to rupture and invade into new erythrocytes, in the absence and presence of peptides (1 or 2). Both peptides significantly inhibited the progression of schizonts to ring stage. The mechanistic details of *Pf*14-3-3I/*Pf*CDPK1 interaction, in context of parasite physiology, has been demonstrated in unpublished data of our group [115]. Since there are no experiments showing that, *in vivo*, the peptides disrupt only *Pf*14-3-3I/*Pf*CDPK1 interaction, the percentage of parasite growth defect could *partly* be due to the abrogation of the interaction of 14-3-3 with its binding partners other than *Pf*CDPK1.

In conclusion, our findings confirm the existence of *Pf*14-3-3I protein in the malaria parasite *P. falciparum*, and present insight into its sequence and structural features which may prove to be an initial lead in understanding its function in the parasite. Moreover, we have shown the physiological relevance of *Pf*14-3-3I/*Pf*CDPK1 interaction in the parasite, as represented schematically in Figure 6. This study would be useful for designing target specific 14-3-3 recognition motif peptides to block the interaction of *Pf*14-3-3I with its partner protein(s), and for developing a potential antimalarial strategy.

Biochemical Journal (2020) **477** 2153–2177
https://doi.org/10.1042/BCJ20200145

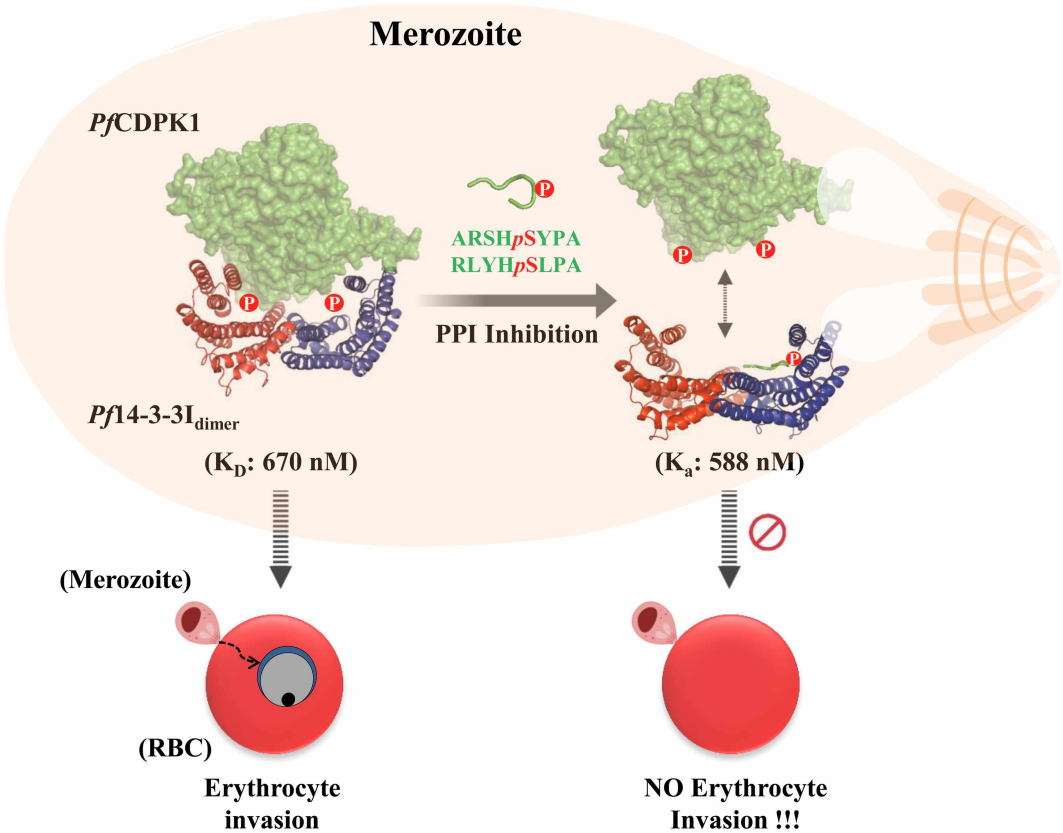

Figure 6. Overall schematic representation.

*Pf*14-3-3I interacts with *Pf*CDPK1 in a phosphorylation dependent manner. Interaction validation with well characterized optimal 14-3-3 recognition motifs: ARSH*p*SYPA (Mode I) and RLYH*p*SLPA (Mode II) indicated that *Pf*14-3-3/*Pf*CDPK1 PPI plays crucial physiological role in the parasite.

Competing Interests

The authors declare that there are no competing interests associated with the manuscript.

Funding

Funding from Science and Engineering Research Board (SERB) (EMR/2016/005644) and Drug and Pharmaceuticals Research Programe (DPRP) (Project No. P/569/2016-1/TDT) for S.S. is acknowledged. S.S. is a recipient of the Innovative Young Biotechnologist Award (IYBA) and National Bioscientist Award from Department of Biotechnology (DBT). R.J. acknowledges University Grant Commission (UGC) for doctoral research fellowship.

Author Contributions

R.J. and S.S. designed the experiments. R.J., P.D. and S.G. performed the experiments. S.P. and S.S. contributed reagents. R.J., A.B., M.M., S.S. analyzed the data. R.J., P.D., A.B. and S.S. wrote the manuscript.

Acknowledgements

Authors acknowledge AutoLab Esprit SPR facility of Advanced Instrumentation Research Facility (AIRF), Jawaharlal Nehru University (JNU), New Delhi, India and Central Instrumentation Facility (CIF) of SCMM, JNU for flow cytometry. The lab facility of Shiv Nadar University is also acknowledged.

Abbreviations

CDPK1, Calcium Dependent Protein Kinase 1; K_a, binding affinity constant; MD, Molecular Dynamics; MSA, Multiple Sequence Alignment; PKA_C, Protein Kinase A catalytic subunit; PKA_R, Protein Kinase A regulatory

Biochemical Journal (2020) **477** 2153–2177
https://doi.org/10.1042/BCJ20200145

subunit; PKG, Protein Kinase G; PPI, Protein–Protein Interaction; PPI, Protein–Protein Interaction; pS/pT, phosphor-Serine/Threonine.

References

1 Wold, F. (1981) In vivo chemical modification of proteins (post-translational modification). *Annu. Rev. Biochem.* **50**, 783–814 https://doi.org/10.1146/annurev.bi.50.070181.004031
2 Olsen J, V., Blagoev, B., Gnad, F., Macek, B., Kumar, C., Mortensen, P. et al. (2006) Global, in vivo, and site-Specific phosphorylation dynamics in signaling networks. *Cell* **127**, 635–648 https://doi.org/10.1016/j.cell.2006.09.026
3 Aitken, A., Collinge, D.B., van Heusden, B.P.H., Isobe, T., Roseboom, P.H., Rosenfeld, G. et al. (1992) 14-3-3 proteins: a highly conserved, widespread family of eukaryotic proteins. *Trends Biochem. Sci.* **17**, 498–501 https://doi.org/10.1016/0968-0004(92)90339-B
4 Fu, H., Subramanian, R.R. and Masters, S.C. (2000) 14-3-3 proteins: structure, function, and regulation. *Annu. Rev. Pharmacol. Toxicol.* **40**, 617–647 https://doi.org/10.1146/annurev.pharmtox.40.1.617
5 Huber, S.C., MacKintosh, C. and Kaiser, W.M. (2002) Metabolic enzymes as targets for 14-3-3 proteins. *Plant Mol. Biol.* **50**, 1053–1063 https://doi.org/10.1023/A:1021284002779
6 Chevalier, D., Morris, E.R. and Walker, J.C. (2009) 14-3-3 and FHA domains mediate phosphoprotein interactions. *Annu. Rev. Plant Biol.* **60**, 67–91 https://doi.org/10.1146/annurev.arplant.59.032607.092844
7 Denison, F.C., Paul, A.L., Zupanska, A.K. and Ferl, R.J. (2011) 14-3-3 proteins in plant physiology. *Semin. Cell Dev. Biol.* **22**, 720–727 https://doi.org/10.1016/j.semcdb.2011.08.006
8 Keicher, J., Jaspert, N., Weckermann, K., Möller, C., Throm, C., Kintzi, A. et al. (2017) Arabidopsis 14-3-3 epsilon members contribute to polarity of PIN auxin carrier and auxin transport-related development. *eLife* **6**, e24336 https://doi.org/10.7554/eLife.24336
9 Paul, A.L., Denison, F.C., Schultz, E.R., Zupanska, A.K. and Ferl, R.J. (2012) 14-3-3 phosphoprotein interaction networks—Does isoform diversity present functional interaction specification? *Front. Plant Sci.* **3**, 190 https://doi.org/10.3389/fpls.2012.00190
10 Rosenquist, M., Sehnke, P., Ferl, R.J., Sommarin, M. and Larsson, C. (2000) Evolution of the 14-3-3 protein family: does the large number of isoforms in multicellular organisms reflect functional specificity? *J. Mol. Evol.* **51**, 446–458 https://doi.org/10.1007/s002390010107
11 Wilson, R.S., Swatek, K.N. and Thelen, J.J. (2016) Regulation of the regulators: post-translational modifications, subcellular, and spatiotemporal distribution of plant 14-3-3 proteins. *Front. Plant Sci.* **7**, 611 https://doi.org/10.3389/fpls.2016.00611
12 Pallucca, R., Visconti, S., Camoni, L., Cesareni, G., Melino, S., Panni, S. et al. (2014) Specificity of ε and non-ε isoforms of Arabidopsis 14-3-3 proteins towards the H+-ATPase and other targets. *PLoS ONE* **9**, e90764 https://doi.org/10.1371/journal.pone.0090764
13 Coblitz, B., Shikano, S., Wu, M., Gabelli, S.B., Cockrell, L.M., Spieker, M. et al. (2005) C-terminal recognition by 14-3-3 proteins for surfase expression of membrane receptors. *J. Biol. Chem.* **280**, 36263–36272 https://doi.org/10.1074/jbc.M507559200
14 Yaffe, M.B., Rittinger, K., Volinia, S., Caron, P.R., Aitken, A., Leffers, H. et al. (1997) The structural basis for 14-3-3:phosphopeptide binding specificity. *Cell* **91**, 961–971 https://doi.org/10.1016/S0092-8674(00)80487-0
15 Muslin, A.J., Tanner, J.W., Allen, P.M. and Shaw, A.S. (1996) Interaction of 14-3-3 with signaling proteins is mediated by the recognition of phosphoserine. *Cell* **84**, 889–897 https://doi.org/10.1016/S0092-8674(00)81067-3
16 Coblitz, B., Wu, M., Shikano, S. and Li, M. (2006) C-terminal binding: an expanded repertoire and function of 14-3-3 proteins. *FEBS Lett.* **580**, 1531–1535 https://doi.org/10.1016/j.febslet.2006.02.014
17 Paiardini, A., Aducci, P., Cervoni, L., Cutruzzolà, F., Di Lucente, C., Janson, G. et al. (2014) The phytotoxin fusicoccin differently regulates 14-3-3 proteins association to mode III targets. *IUBMB Life* **66**, 52–62 https://doi.org/10.1002/iub.1239
18 Kilisch, M., Lytovchenko, O., Arakel, E.C., Bertinetti, D. and Schwappach, B. (2016) A dual phosphorylation switch controls 14-3-3-dependent cell surface expression of TASK-1. *J. Cell Sci.* **129**, 831–842 https://doi.org/10.1242/jcs.180182
19 Tzivion, G., Luo, Z. and Avruch, J. (1998) A dimeric.14-3-3 protein is an essential cofactor for Raf kinase activity. *Nature* **394**, 88–92 https://doi.org/10.1038/27938
20 Obsil, T., Ghirlando, R., Klein, D.C., Ganguly, S. and Dyda, F. (2001) Crystal structure of the 14-3-3ζ:serotonin N-acetyltransferase complex: a role for scaffolding in enzyme regulation. *Cell* **105**, 257–267 https://doi.org/10.1016/S0092-8674(01)00316-6
21 Mackintosh, C. (2004) Dynamic interactions between 14-3-3 proteins and phosphoproteins regulate diverse cellular processes. *Biochem. J.* **381**, 329–342 https://doi.org/10.1042/BJ20031332
22 Yaffe, M.B. (2002) How do 14-3-3 proteins work?—Gatekeeper phosphorylation and the molecular anvil hypothesis. *FEBS Lett.* **513**, 53–57 https://doi.org/10.1016/S0014-5793(01)03288-4
23 Hermeking, H. (2003) The 14-3-3 cancer connection. *Nat. Rev. Cancer* **3**, 931–943 https://doi.org/10.1038/nrc1230
24 Aitken, A. (1996) 14-3-3 and its possible role in co-ordinating multiple signalling pathways. *Trends Cell Biol.* **6**, 341–347 https://doi.org/10.1016/0962-8924(96)10029-5
25 Tzivion, G., Shen, Y.H. and Zhu, J. (2001) 14-3-3 proteins; bringing new definitions to scaffolding. *Oncogene* **20**, 6331–6338 https://doi.org/10.1038/sj.onc.1204777
26 Van Hemert, M.J., Yde Steensma, H. and Van Paul, G. (2001) 14-3-3 proteins: key regulators of cell division, signalling and apoptosis. *BioEssays* **23**, 936–946 https://doi.org/10.1002/bies.1134
27 Wilker, E. and Yaffe, M.B. (2004) 14-3-3 proteins—A focus on cancer and human disease. *J. Mol. Cell Cardiol.* **37**, 633–642 https://doi.org/10.1016/j.yjmcc.2004.04.015
28 Kundu, A., Shelar, S., Ghosh, A., Ballestas, M., Kirkman, R., Nam, H.Y. et al. (2020) 14-3-3 proteins protect AMPK-phosphorylated ten-eleven translocation-2 (TET2) from PP2A-mediated dephosphorylation. *J. Biol. Chem.* **295**, 1754–1766 https://doi.org/10.1074/jbc.RA119.011089
29 Rittinger, K., Budman, J., Xu, J., Volinia, S., Cantley, L.C., Smerdon, S.J. et al. (1999) Structural analysis of 14-3-3 phosphopeptide complexes identifies a dual role for the nuclear export signal of 14-3-3 in ligand binding. *Mol. Cell* **4**, 153–166 https://doi.org/10.1016/S1097-2765(00)80363-9
30 Trager, W. and Jensen, J.B. (1976) Human malaria parasites in continuous culture. *Science* **193**, 673–675 https://doi.org/10.1126/science.781840
31 Bateman, A. (2019) Uniprot: a worldwide hub of protein knowledge. *Nucleic Acids Res.* **47**, D506–D515 https://doi.org/10.1093/nar/gky1049

32 Aurrecoechea, C., Brestelli, J., Brunk, B.P., Dommer, J., Fischer, S., Gajria, B. et al. (2009) PlasmoDB: a functional genomic database for malaria parasites. *Nucleic Acids Res.* **37**, D539–D543 https://doi.org/10.1093/nar/gkn814
33 Corpet, F. (1988) Multiple sequence alignment with hierarchical clustering. *Nucleic Acids Res.* **16**, 10881–10890 https://doi.org/10.1093/nar/16.22.10881
34 Wang, W. and Shakes, D.C. (1996) Molecular evolution of the 14-3-3 protein family. *J. Mol. Evol.* **43**, 384–398 https://doi.org/10.1007/BF02339012
35 Gardino, A.K., Smerdon, S.J. and Yaffe, M.B. (2006) Structural determinants of 14-3-3 binding specificities and regulation of subcellular localization of 14-3-3-ligand complexes: a comparison of the X-ray crystal structures of all human 14-3-3 isoforms. *Semin. Cancer Biol.* **16**, 173–182 https://doi.org/10.1016/j.semcancer.2006.03.007
36 Wilkert, E.W., Grant, R.A., Artim, S.C. and Yaffe, M.B. (2005) A structural basis for 14-3-3σ functional specificity. *J. Biol. Chem.* **280**, 18891–18898 https://doi.org/10.1074/jbc.M500982200
37 Liu, W., Xie, Y., Ma, J., Luo, X., Nie, P., Zuo, Z. et al. (2015) IBS: an illustrator for the presentation and visualization of biological sequences. *Bioinformatics* **31**, 3359–3361 https://doi.org/10.1093/bioinformatics/btv362
38 Berardini, T.Z., Reiser, L., Li, D., Mezheritsky, Y., Muller, R., Strait, E. et al. (2015) The Arabidopsis information resource: making and mining the 'gold standard' annotated reference plant genome. *Genesis* **53**, 474–485 https://doi.org/10.1002/dvg.22877
39 Van Heusden, G.P.H., Griffiths, D.J.F., Ford, J.C., Chin-A-Woeng, T.F.C., Schrader, P.A.T., Carr, A.M. et al. (1995) The 14-3-3 proteins encoded by the BMH1 and BMH2 genes are essential in the yeast *Saccharomyces cerevisiae* and Can be replaced by a plant homologue. *Eur. J. Biochem.* **229**, 45–53 https://doi.org/10.1111/j.1432-1033.1995.0045l.x
40 Xu, W.F. and Shi, W.M. (2006) Expression profiling of the 14-3-3 gene family in response to salt stress and potassium and iron deficiencies in young tomato (Solanum lycopersicum) roots: analysis by real-time RT-PCR. *Ann. Bot.* **98**, 965–974 https://doi.org/10.1093/aob/mcl189
41 Tian, F., Wang, T., Xie, Y., Zhang, J. and Hu, J. (2015) Genome-wide identification, classification, and expression analysis of 14-3-3 gene family in populus. *PLoS ONE* **10**, e0123225 https://doi.org/10.1371/journal.pone.0123225
42 Tamura, K., Stecher, G., Peterson, D., Filipski, A. and Kumar, S. (2013) MEGA6: molecular evolutionary genetics analysis version 6.0. *Mol. Biol. Evol.* **30**, 2725–2729 https://doi.org/10.1093/molbev/mst197
43 Dinkel, H., Michael, S., Weatheritt, R.J., Davey, N.E., Van Roey, K., Altenberg, B. et al. (2012) ELM—The database of eukaryotic linear motifs. *Nucleic Acids Res.* **40**, D242–D251 https://doi.org/10.1093/nar/gkr1064
44 Tinti, M., Madeira, F., Murugesan, G., Hoxhaj, G., Toth, R. and MacKintosh, C. (2014) ANIA: ANnotation and integrated analysis of the 14-3-3 interactome. *Database* **2014**, bat085 https://doi.org/10.1093/database/bat085
45 Johnson, C., Crowther, S., Stafford, M.J., Campbell, D.G., Toth, R. and MacKintosh, C. (2010) Bioinformatic and experimental survey of 14-3-3-binding sites. *Biochem. J.* **427**, 69–78 https://doi.org/10.1042/BJ20091834
46 Madeira, F., Tinti, M., Murugesan, G., Berrett, E., Stafford, M., Toth, R. et al. (2015) 14-3-3-Pred: improved methods to predict 14-3-3-binding phosphopeptides. *Bioinformatics* **31**, 2276–2283 https://doi.org/10.1093/bioinformatics/btv133
47 Pozuelo-Rubio, M. (2010) Proteomic and biochemical analysis of 14-3-3-binding proteins during C2-ceramide-induced apoptosis. *FEBS J.* **277**, 3321–3342 https://doi.org/10.1111/j.1742-4658.2010.07730.x
48 Crooks, G.E., Hon, G., Chandonia, J.M. and Brenner, S.E. (2004) Weblogo: a sequence logo generator. *Genome Res.* **14**, 1188–1190 https://doi.org/10.1101/gr.849004
49 Treeck, M., Sanders, J.L., Elias, J.E. and Boothroyd, J.C. (2011) The phosphoproteomes of *Plasmodium falciparum* and *Toxoplasma gondii* reveal unusual adaptations within and beyond the parasites' boundaries. *Cell Host Microbe* **10**, 410–419 https://doi.org/10.1016/j.chom.2011.09.004
50 Solyakov, L., Halbert, J., Alam, M.M., Semblat, J.P., Dorin-Semblat, D., Reininger, L. et al. (2011) Global kinomic and phospho-proteomic analyses of the human malaria parasite *Plasmodium falciparum*. *Nat. Commun.* **2**, 565 https://doi.org/10.1038/ncomms1558
51 Lasonder, E., Green, J.L., Camarda, G., Talabani, H., Holder, A.A., Langsley, G. et al. (2012) The plasmodium falciparum schizont phosphoproteome reveals extensive phosphatidylinositol and cAMP-protein kinase A signaling. *J. Proteome Res.* **11**, 5323–5337 https://doi.org/10.1021/pr300557m
52 Alam, M.M., Solyakov, L., Bottrill, A.R., Flueck, C., Siddiqui, F.A., Singh, S. et al. (2015) Phosphoproteomics reveals malaria parasite protein kinase G as a signalling hub regulating egress and invasion. *Nat. Commun.* **6**, 7285 https://doi.org/10.1038/ncomms8285
53 Kumar, S., Kumar, M., Ekka, R., Dvorin, J.D., Paul, A.S., Madugundu, A.K. et al. (2017) PfCDPK1 mediated signaling in erythrocytic stages of plasmodium falciparum. *Nat. Commun.* **8**, 63 https://doi.org/10.1038/s41467-017-00053-1
54 Bansal, A., Singh, S., More, K.R., Hans, D., Nangalia, K., Yogavel, M. et al. (2013) Characterization of plasmodium falciparum calcium-dependent protein kinase 1 (PFCDPK1) and its role in microneme secretion during erythrocyte invasion. *J. Biol. Chem.* **288**, 1590–1602 https://doi.org/10.1074/jbc.M112.411934
55 Dangi, P., Jain, R., Mamidala, R., Sharma, V., Agarwal, S., Bathula, C. et al. (2019) Natural product inspired novel indole based chiral scaffold kills human malaria parasites via ionic imbalance mediated cell death. *Sci. Rep.* **9**, 17785 https://doi.org/10.1038/s41598-019-54339-z
56 Altschul, S.F., Gish, W., Miller, W., Myers, E.W. and Lipman, D.J. (1990) Basic local alignment search tool. *J. Mol. Biol.* **215**, 403–410 https://doi.org/10.1016/S0022-2836(05)80360-2
57 Berman, H.M., Westbrook, J., Feng, Z., Gilliland, G., Bhat, T.N., Weissig, H. et al. (2000) The protein data bank. *Nucleic Acids Res.* **28**, 235–242 https://doi.org/10.1093/nar/28.1.235
58 Molzan, M., Weyand, M., Rose, R. and Ottmann, C. (2012) Structural insights of the MLF1/14-3-3 interaction. *FEBS J.* **279**, 563–571 https://doi.org/10.1111/j.1742-4658.2011.08445.x
59 Wernimont, A.K., Hutchinson, A., Sullivan, H., Panico, E., Crombet, L., Cossar, D. et al. Crystal Structure of CDPK1 from *Plasmodium Bergheii*, PBANKA_031420; To be published
60 Jain, R., Gupta, S., Munde, M. and Pati SS, S. (2020) Development of novel anti-Malarial from structurally diverse library of molecules, targeting plant-Like CDPK1, a multistage growth regulator of *P. falciparum*. *Biochem. J.* **477**, 1951–1970 https://doi.org/10.1042/BCJ20200045
61 Webb, B. and Sali, A. (2016) Comparative protein structure modeling using MODELLER. *Curr. Protoc. Bioinformatics* **54**, 5.6.1–5.6.37 https://doi.org/10.1002/cpbi.3
62 *The PyMOL Molecular Graphics System, Version 2.1*, Schrödinger, LLC

Biochemical Journal (2020) **477** 2153–2177
https://doi.org/10.1042/BCJ20200145

63 Xu, D. and Zhang, Y. (2011) Improving the physical realism and structural accuracy of protein models by a two-step atomic-level energy minimization. *Biophys. J.* **101**, 2525–2534 https://doi.org/10.1016/j.bpj.2011.10.024

64 Ramachandran, G.N. and Sasisekharan, V. (1968) Conformation of polypeptides and proteins. *Adv. Protein Chem.* **23**, 283–437 https://doi.org/10.1016/S0065-3233(08)60402-7

65 Laskowski, R.A., MacArthur, M.W. and Thornton, J.M. (1993) PROCHECK: a program to check the stereochemical quality of protein structures. *J. Appl. Crystallogr.* **26**, 283–291 https://doi.org/10.1107/S0021889892009944

66 Morris, G.M., Ruth, H., Lindstrom, W., Sanner, M.F., Belew, R.K., Goodsell, D.S. et al. (2009) Autodock4 and AutoDockTools4: automated docking with selective receptor flexibility. *J. Comput. Chem.* **30**, 2785–2791 https://doi.org/10.1002/jcc.21256

67 Dominguez, C., Boelens, R. and Bonvin, A.M.J.J. (2003) HADDOCK: a protein-protein docking approach based on biochemical or biophysical information. *J. Am. Chem. Soc.* **125**, 1731–1737 https://doi.org/10.1021/ja026939x

68 Ahmed, A., Gaadhe, K., Sharma, G.P., Kumar, N., Neculai, M., Hui, R. et al. (2012) Novel insights into the regulation of malarial calcium-dependent protein kinase 1. *FASEB J.* **26**, 3212–3221 https://doi.org/10.1096/fj.12-203877

69 Warnecke, A., Sandalova, T., Achour, A. and Harris, R.A. (2014) PyTMs: a useful PyMOL plugin for modeling common post-translational modifications. *BMC Bioinformatics* **15**, 370 https://doi.org/10.1186/s12859-014-0370-6

70 Case, D.A., Babin, V., Berryman, J.T., Betz, R.M., Cai, Q., Cerutti, D.S., et al. (2014) *AMBER 14*, University of California, San Francisco

71 Duan, Y., Wu, C., Chowdhury, S., Lee, M.C., Xiong, G., Zhang, W. et al. (2003) A point-charge force field for molecular mechanics simulations of proteins based on condensed-Phase quantum mechanical calculations. *J. Comput. Chem.* **24**, 1999–2012 https://doi.org/10.1002/jcc.10349

72 Khoury, G.A., Thompson, J.P., Smadbeck, J., Kieslich, C.A. and Floudas, C.A. (2013) Forcefield-PTM: ab initio charge and AMBER forcefield parameters for frequently occurring post-translational modifications. *J. Chem. Theory Comput.* **9**, 5653–5674 https://doi.org/10.1021/ct400556v

73 Ryckaert, J.P., Ciccotti, G. and Berendsen, H.J.C. (1977) Numerical integration of the cartesian equations of motion of a system with constraints: molecular dynamics of n-alkanes. *J. Comput. Phys.* **23**, 327–341 https://doi.org/10.1016/0021-9991(77)90098-5

74 Darden, T., York, D. and Pedersen, L. (1993) Particle mesh Ewald: an N·log(N) method for Ewald sums in large systems. *J. Chem. Phys.* **98**, 10089 https://doi.org/10.1063/1.464397

75 Genheden, S. and Ryde, U. (2015) The MM/PBSA and MM/GBSA methods to estimate ligand-binding affinities. *Expert Opin. Drug Discov.* **10**, 449–461 https://doi.org/10.1517/17460441.2015.1032936

76 Miller, B.R., McGee, T.D., Swails, J.M., Homeyer, N., Gohlke, H. and Roitberg, A.E. (2012) MMPBSA.py: an efficient program for end-state free energy calculations. *J. Chem. Theory Comput.* **8**, 3314–3321 https://doi.org/10.1021/ct300418h

77 Jain, R., Garg, S. and Singh, S. (2019) Screening of chemical library against whole cell kinome activity via non-radioactive, high throughput kinase assay. *MethodsX.* **6**, 162–168 https://doi.org/10.1016/j.mex.2018.12.003

78 Hans, N., Singh, S., Pandey, A.K., Reddy, K.S., Gaur, D. and Chauhan, V.S. (2013) Identification and characterization of a novel *Plasmodium falciparum* adhesin involved in erythrocyte invasion. *PLoS ONE* **8**, e74790 https://doi.org/10.1371/journal.pone.0074790

79 Matta, S.K., Agarwal, S. and Bhatnagar, R. (2010) Surface localized and extracellular glyceraldehyde-3-phosphate dehydrogenase of *Bacillus anthracis* is a plasminogen binding protein. *Biochim. Biophys. Acta* **1804**, 2111–2120 https://doi.org/10.1016/j.bbapap.2010.08.004

80 Rehman, S.A.A., Verma, V., Mazumder, M., Dhar, S.K. and Gourinath, S. (2013) Crystal structure and mode of helicase binding of the C-terminal domain of primase from *Helicobacter pylori*. *J. Bacteriol.* **195**, 2826–2838 https://doi.org/10.1128/JB.00091-13

81 Pandey, P., Tarique, K.F., Mazumder, M., Rehman, S.A.A., Kumari, N. and Gourinath, S. (2016) Structural insight into β-Clamp and its interaction with DNA ligase in *Helicobacter pylori*. *Sci. Rep.* **6**, 31181 https://doi.org/10.1038/srep31181

82 Tiwari, N., Srivastava, A., Kundu, B. and Munde, M. (2018) Biophysical insight into the heparin-peptide interaction and its modulation by a small molecule. *J. Mol. Recognit.* **31**, e2674 https://doi.org/10.1002/jmr.2674

83 Rahi, A., Matta, S.K., Dhiman, A., Garhyan, J., Gopalani, M., Chandra, S. et al. (2017) Enolase of *Mycobacterium tuberculosis* is a surface exposed plasminogen binding protein. *Biochim. Biophys. Acta Gen. Subj.* **1861**, 3355–3364 https://doi.org/10.1016/j.bbagen.2016.08.018

84 Tanwar, N. and Munde, M. (2018) Thermodynamic and conformational analysis of the interaction between antibody binding proteins and IgG. *Int. J. Biol. Macromol.* **112**, 1084–1092 https://doi.org/10.1016/j.ijbiomac.2018.01.208

85 Gupta, S., Tiwari, N. and Munde, M. (2019) A comprehensive biophysical analysis of the effect of DNA binding drugs on protamine-induced DNA condensation. *Sci. Rep.* **9**, 5891 https://doi.org/10.1038/s41598-019-41975-8

86 Imam, M., Singh, S., Kaushik, N.K. and Chauhan, V.S. (2014) *Plasmodium falciparum* merozoite surface protein 3: oligomerization, self-assembly, and heme complex formation. *J. Biol. Chem.* **289**, 3856–3868 https://doi.org/10.1074/jbc.M113.520239

87 Wang, B., Yang, H., Liu, Y.C., Jelinek, T., Zhang, L., Ruoslahti, E. et al. (1999) Isolation of high-affinity peptide antagonists of 14-3-3 proteins by phage display. *Biochemistry* **38**, 12499–12504 https://doi.org/10.1021/bi991353h

88 Petosa, C., Masters, S.C., Bankston, L.A., Pohl, J., Wang, B., Fu, H. et al. (1998) 14-3-3ζ binds a phosphorylated raf peptide and an unphosphorylated peptide via its conserved amphiphatic groove. *J. Biol. Chem.* **273**, 16305–16310 https://doi.org/10.1074/jbc.273.26.16305

89 Masters, S.C. and Fu, H. (2001) 14-3-3 proteins mediate an essential anti-apoptotic signal. *J. Biol. Chem.* **276**, 45193–45200 https://doi.org/10.1074/jbc.M105971200

90 Glas, A., Bier, D., Hahne, G., Rademacher, C., Ottmann, C. and Grossmann, T.N. (2014) Constrained peptides with target-adapted cross-links as inhibitors of a pathogenic protein-protein interaction. *Angew. Chem. Int. Ed. Engl.* **53**, 2489–2493 https://doi.org/10.1002/anie.201310082

91 Cromm, P.M., Wallraven, K., Glas, A., Bier, D., Fürstner, A., Ottmann, C. et al. (2016) Constraining an irregular peptide secondary structure through ring-Closing alkyne metathesis. *ChemBioChem.* **17**, 1915–1919 https://doi.org/10.1002/cbic.201600362

92 Milroy, L.G., Bartel, M., Henen, M.A., Leysen, S., Adriaans, J.M.C., Brunsveld, L. et al. (2015) Stabilizer-Guided inhibition of protein-Protein interactions. *Angew. Chem. Int. Ed. Engl.* **54**, 15720–4 https://doi.org/10.1002/anie.201507976

93 Velazquez-Campoy, A., Todd, M.J. and Freire, E. (2000) HIV-1 protease inhibitors: enthalpic versus entropic optimization of the binding affinity. *Biochemistry* **39**, 2201–2207 https://doi.org/10.1021/bi992399d

94 Al-Khedery, B., Barnwell, J.W. and Galinski, M.R. (1999) Stage-specific expression of 14-3-3 in asexual blood-stage plasmodium. *Mol. Biochem. Parasitol.* **102**, 117–130 https://doi.org/10.1016/S0166-6851(99)00090-0

95 Lalle, M., Currà, C., Ciccarone, F., Pace, T., Cecchetti, S., Fantozzi, L. et al. (2011) Dematin, a component of the erythrocyte membrane skeleton, is internalized by the malaria parasite and associates with *Plasmodium* 14-3-3. *J. Biol. Chem.* **286**, 1227–1236 https://doi.org/10.1074/jbc.M110.194613
96 Dastidar, E.G. Dzeyk, K., Krijgsveld, J., Malmquist, N.A., Doerig, C., Scherf, A. et al. (2013) Comprehensive histone phosphorylation analysis and identification of Pf14-3-3 protein as a histone H3 phosphorylation reader in malaria parasites. *PLoS ONE* **8**, e53179 https://doi.org/10.1371/journal.pone.0053179
97 Ferl, R.J., Manak, M.S. and Reyes, M.F. (2002) The 14-3-3s. *Genome Biol.* **3**, reviews3010.1 https://doi.org/10.1186/gb-2002-3-7-reviews3010
98 Aitken, A., Ellis, C.A., Harris, A., Sellers, L.A. and Toker, A. (1990) Kinase and neurotransmitters. *Nature* **344**, 594 https://doi.org/10.1038/344594a0
99 Toker, A., Ellis, C.A., Sellers, L.A. and Aitken, A. (1990) Protein kinase C inhibitor proteins: purification from sheep brain and sequence similarity to lipocortins and 14-3-3 protein. *Eur. J. Biochem.* **191**, 421–429 https://doi.org/10.1111/j.1432-1033.1990.tb19138.x
100 Toker, A., Sellers, L.A., Amess, B., Patel, Y., Harris, A. and Aitken, A. (1992) Multiple isoforms of a protein kinase C inhibitor (KCIP-1/14-3-3) from sheep brain: amino acid sequence of phosphorylated forms. *Eur. J. Biochem.* **206**, 453–461 https://doi.org/10.1111/j.1432-1033.1992.tb16946.x
101 Robinson, K., Jones, D., Patel, Y., Martin, H., Madrazo, J., Martin, S. et al. (1994) Mechanism of inhibition of protein kinase C by 14-3-3 isoforms. 14-3-3 isoforms do not have phospholipase A2 activity. *Biochem. J.* **299**, 853–861 https://doi.org/10.1042/bj2990853
102 Wheeler-Jones, C.P.D., Learmonth, M.P., Martin, H. and Aitken, A. (1996) Identification of 14-3-3 proteins in human platelets: effects of synthetic peptides on protein kinase C activation. *Biochem. J.* **315**, 41–47 https://doi.org/10.1042/bj3150041
103 Hausser, A., Storz, P., Link, G., Stoll, H., Liu, Y.C., Altman, A. et al. (1999) Protein kinase C μ is negatively regulated by 14-3-3 signal transduction proteins. *J. Biol. Chem.* **274**, 9258–9264 https://doi.org/10.1074/jbc.274.14.9258
104 Isobe, T., Hiyane, Y., Ichimura, T., Okuyama, T., Takahashi, N., Nakajo, S. et al. (1992) Activation of protein kinase C by the 14-3-3 proteins homologous with Exol protein that stimulates calcium-dependent exocytosis. *FEBS Lett.* **308**, 121–124 https://doi.org/10.1016/0014-5793(92)81257-M
105 Tanji, M., Horwitz, R., Rosenfeld, G. and Waymire, J.C. (1994) Activation of protein kinase C by purified bovine brain 14-3-3: comparison with tyrosine hydroxylase activation. *J. Neurochem.* **63**, 1908–1916 https://doi.org/10.1046/j.1471-4159.1994.63051908.x
106 Acs, P., Szallasi, Z., Kazanietz, M.G. and Blumberg, P.M. (1995) Differential activation of PKC isozymes by 14-3-3 ζ protein. *Biochem. Biophys. Res. Commun.* **216**, 103–109 https://doi.org/10.1006/bbrc.1995.2597
107 Fantl, W.J., Muslin, A.J., Kikuchi, A., Martin, J.A., MacNicol, A.M., Grosst, R.W. et al. (1994) Activation of Raf-1 by 14-3-3 proteins. *Nature* **371**, 612–614 https://doi.org/10.1038/371612a0
108 Takihara, Y., Matsuda, Y. and Hara, J. (2000) Role of the beta isoform of 14-3-3 proteins in cellular proliferation and oncogenic transformation. *Carcinogenesis* **21**, 2073–2077 https://doi.org/10.1093/carcin/21.11.2073
109 Rothblum-Oviatt, C.J., Ryan, C.E. and Piwnica-Worms, H. (2001) 14-3-3 binding regulates catalytic activity of human Wee1 kinase. *Cell Growth Differ.* **12**, 581–589 PMID:11751453
110 Kim, D., Won, J., Shin, D.W., Kang, J., Kim, Y.J., Choi, S.Y. et al. (2004) Regulation of Dyrk1A kinase activity by 14-3-3. *Biochem. Biophys. Res. Commun.* **323**, 499–504 https://doi.org/10.1016/j.bbrc.2004.08.102
111 Fischer, A., Baljuls, A., Reinders, J., Nekhoroshkova, E., Sibilski, C., Metz, R. et al. (2009) Regulation of RAF activity by 14-3-3 proteins: RAF kinases associate functionally with both homo- and heterodimeric forms of 14-3-3 proteins. *J. Biol. Chem.* **284**, 3183–3194 https://doi.org/10.1074/jbc.M804795200
112 Yuasa, K., Ota, R., Matsuda, S., Isshiki, K., Inoue, M. and Tsuji, A. (2015) Suppression of death-associated protein kinase 2 by interaction with 14-3-3 proteins. *Biochem. Biophys. Res. Commun.* **464**, 70–75 https://doi.org/10.1016/j.bbrc.2015.05.105
113 Bhattacherjee, A. and Wallin, S. (2013) Exploring protein-Peptide binding specificity through computational peptide screening. *PLoS Comput. Biol.* **9**, e1003277 https://doi.org/10.1371/journal.pcbi.1003277
114 Bhattacherjee, A. and Wallin, S. (2012) Coupled folding-binding in a hydrophobic/polar protein model: impact of synergistic folding and disordered flanks. *Biophys. J.* **102**, 569–578 https://doi.org/10.1016/j.bpj.2011.12.008
115 More, K.R., Kaur, I., Gianetto, Q.G., Invergo, B.M., Chaze, T., Jain, R. et al. (2020) Phosphorylation-Dependent assembly of a 14-3-3 mediated signaling complex during Red blood cell invasion by plasmodium falciparum merozoites. *bioRxiv* https://doi.org/10.1101/2020.01.17.911107